RESEARCH ARTICLE

The Polyamine–Hypusine Circuit Controls an Oncogenic Translational Program Essential for Malignant Conversion in MYC-Driven Lymphoma

Shima Nakanishi[1], Jiannong Li[2], Anders E. Berglund[2], Youngchul Kim[2], Yonghong Zhang[2], Ling Zhang[3], Chunying Yang[1], Jinming Song[3], Raghavendra G. Mirmira[4], and John L. Cleveland[1]

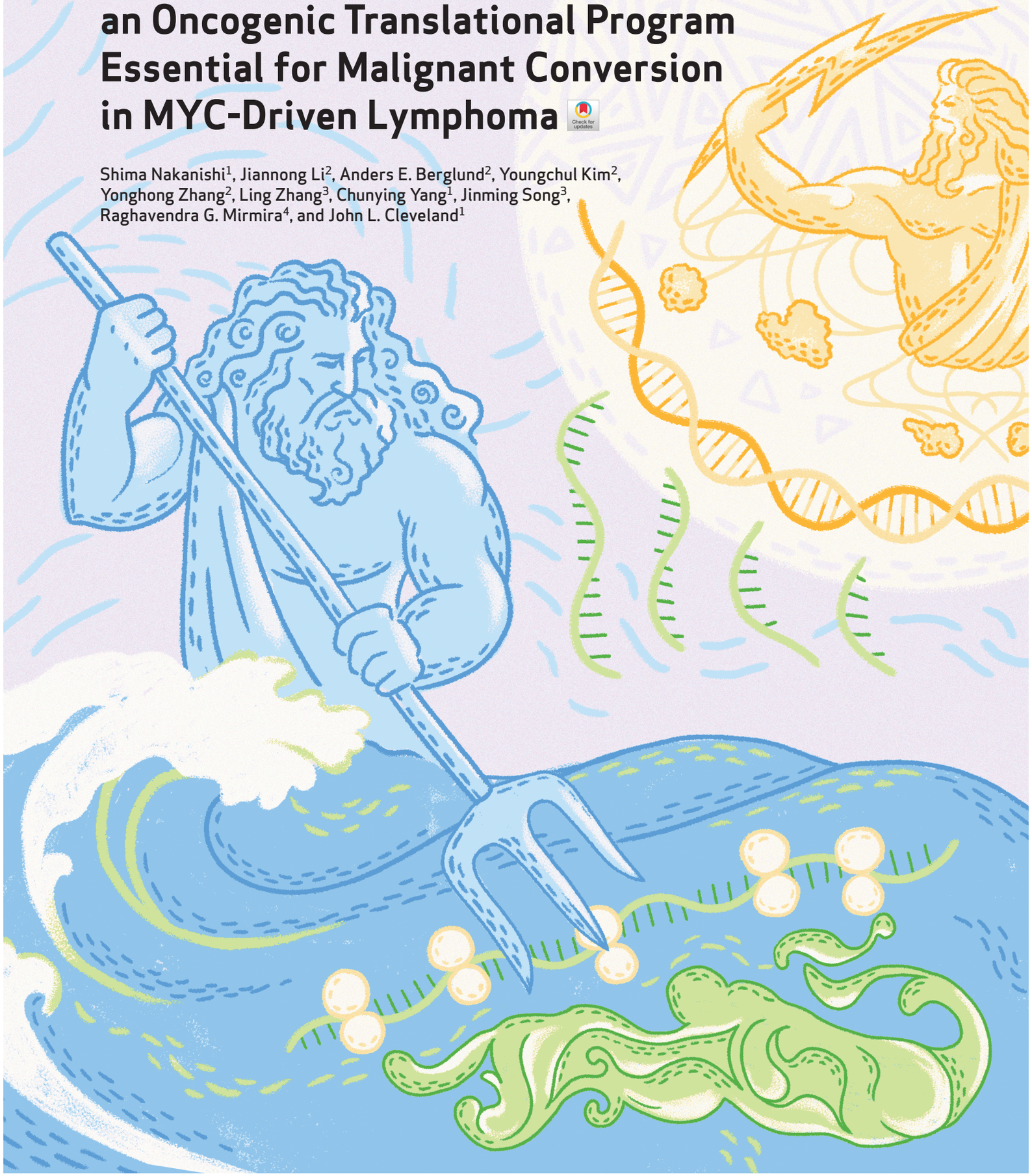

ABSTRACT The *MYC* oncoprotein is activated in a broad spectrum of human malignancies and transcriptionally reprograms the genome to drive cancer cell growth. Given this, it is unclear if targeting a single effector of MYC will have therapeutic benefit. MYC activates the polyamine–hypusine circuit, which posttranslationally modifies the eukaryotic translation factor eIF5A. The roles of this circuit in cancer are unclear. Here we report essential intrinsic roles for hypusinated eIF5A in the development and maintenance of MYC-driven lymphoma, where the loss of eIF5A hypusination abolishes malignant transformation of MYC-overexpressing B cells. Mechanistically, integrating RNA sequencing, ribosome sequencing, and proteomic analyses revealed that efficient translation of select targets is dependent upon eIF5A hypusination, including regulators of G_1–S phase cell-cycle progression and DNA replication. This circuit thus controls MYC's proliferative response, and it is also activated across multiple malignancies. These findings suggest the hypusine circuit as a therapeutic target for several human tumor types.

SIGNIFICANCE: Elevated *EIF5A* and the polyamine–hypusine circuit are manifest in many malignancies, including MYC-driven tumors, and eIF5A hypusination is necessary for MYC proliferative signaling. Notably, this circuit controls an oncogenic translational program essential for the development and maintenance of MYC-driven lymphoma, supporting this axis as a target for cancer prevention and treatment.

See related commentary by Wilson and Klein, p. 248.

INTRODUCTION

MYC family oncoproteins are activated in a broad spectrum of human malignancies (1). However, MYC overexpression alone is not sufficient for the neoplastic transformation of normal human cells and additional cooperating events are necessary (e.g., loss of the tumor suppressor p53 or overexpression of the oncoprotein BCL-2). During cancer progression, MYC-overexpressing cells evolve by various means to bypass cell-cycle and apoptotic checkpoints and, as evidenced by the number and combination of mutations found in aggressive MYC-driven cancers (2), these tumors are particularly challenging to treat. Thus, finding a common MYC downstream effector that controls select factors/pathways (e.g., cell-cycle regulation, ribosome biogenesis, and metabolism) at a posttranscriptional level and that is required for MYC-induced tumorigenesis would be of great interest and should have broad therapeutic benefit.

One MYC-regulated metabolic pathway that appears nearly universally upregulated in cancer is polyamine biosynthesis, which directs the production of putrescine, spermidine, and spermine. Notably, polyamine levels are generally elevated in tumors (3, 4), and targeting the first enzyme of the pathway, ornithine decarboxylase (ODC), impairs the development of MYC-driven lymphoma and MYCN-driven neuroblastoma (5–7). Furthermore, the ODC suicide inhibitor α-difluoromethylornithine (DFMO) has shown activity as a chemoprevention agent in colorectal and prostate cancer trials (8, 9). However, DFMO has little activity as a single agent in cancer therapeutic trials (10), and this likely reflects the fact that polyamines are abundant in the diet and their intracellular levels can be restored by polyamine transport (11).

Interestingly, the 4-aminobutyl moiety of the polyamine spermidine is used as the sole substrate to posttranslationally modify a single lysine residue (Lys-50) of eIF5A (eIF5A1) and eIF5A2 in a process coined hypusination. This two-step conversion is directed by deoxyhypusine synthase (DHPS) and deoxyhypusine hydroxylase (DOHH), which covalently modify $eIF5A^{Lys50}$ with a unique amino acid, hypusine (12). eIF5A was initially identified as a translation initiation factor (13) and has been shown to play additional roles in translation elongation and termination in yeast (14, 15) as well as in start codon selection (16). Furthermore, hypusination of yeast eIF5A augments the translation of mRNAs containing consecutive (>3) polyproline (poly-P) codons (17). Finally, functional roles for hypusinated eIF5A ($eIF5A^{Hyp}$) have been linked to several physiologic processes, including preventing premature aging of the brain (18) and immune senescence (19), as well as in macrophage activation (20), and meta-inflammation (21).

The roles of the polyamine–hypusine circuit in cancer are currently controversial (22), where eIF5A has been suggested to play oncogenic roles in some contexts (23) and to function as a tumor suppressor in others (24, 25). To understand tumor cell–intrinsic effects of the hypusine circuit on tumorigenesis, we targeted the pathway specifically in the B cells of Eμ-*Myc* transgenic mice, a validated model for human B-cell

[1]Department of Tumor Biology, H. Lee Moffitt Cancer Center and Research Institute, Tampa, Florida. [2]Department of Bioinformatics and Biostatistics, H. Lee Moffitt Cancer Center and Research Institute, Tampa, Florida. [3]Department of Pathology and Laboratory Medicine, H. Lee Moffitt Cancer Center and Research Institute, Tampa, Florida. [4]Department of Medicine, The University of Chicago, Chicago, Illinois.

Corresponding Authors: John L. Cleveland, Department of Tumor Biology, Moffitt Cancer Center, Tampa, FL 33612. Phone: 813-745-3888; E-mail: John.Cleveland@moffitt.org; and Shima Nakanishi, Shima.Nakanishi@moffitt.org

Blood Cancer Discov 2023;4:294–317

doi: 10.1158/2643-3230.BCD-22-0162

lymphoma with *MYC* involvement (26). Here we report that hypusinated eIF5A plays critical roles in the maintenance of MYC-driven lymphoma and that DHPS has essential roles in malignant conversion that is necessary for lymphoma development. Further, unbiased global analyses of changes in gene expression, translation, and steady-state protein levels reveal that hypusination of eIF5A controls cell cycle and oncogenic programs that are necessary for lymphoma cell growth.

RESULTS

Activation of the Polyamine–Hypusine Circuit Is a Hallmark of Cancer

To assess the status of the hypusine circuit (Fig. 1A) in cancer in an unbiased fashion, genetic alterations and expression profiles of the genes involved in this process—*EIF5A*, *EIF5A2*, *DHPS*, and *DOHH*—were determined using publicly available data from The Cancer Genome Atlas (TCGA). Deep deletion (−2) or amplification (+2) is rare in *EIF5A*, *DHPS*, and *DOHH* (Supplementary Fig. S1A), although loss of heterozygosity (LOH) in the region of chromosome 17p that harbors the *EIF5A* and/or *TP53* genes is frequent in many tumors (refs. 27–29; Fig. 1B, shallow deletion −1: orange). However, expression analyses across all cancer types revealed that *EIF5A* is significantly overexpressed in many cancers (12/17) compared with corresponding normal tissues, along with *DOHH* (16/17), and that there are modest increases in *DHPS* (8/17) expression in many tumor types (Fig. 1C; Supplementary Fig. S1B). Furthermore, analyses of *EIF5A* expression in the 12 *EIF5A*-overexpressing tumor types with respect to copy-number status revealed that *EIF5A* expression in tumors with shallow deletion is still higher than or equivalent to *EIF5A* expression in normal tissues (Fig. 1D). In contrast, due to a common amplification of chromosome 3q (30), *EIF5A2* (at 3q26.2) is significantly amplified in some cancers including lung squamous (36%) and ovarian cancer (23%) (Supplementary Fig. S1A), and increased *EIF5A2* expression is limited to cancers with 3q26 amplicons (Fig. 1C).

Previously, we and others have shown that the polyamine biosynthetic genes *ODC1*, *AMD1*, and *SRM* are direct transcription targets of MYC (Fig. 1A; ref. 5), and their expression correlates well with *MYC* expression across cancer types (Supplementary Fig. S1C). Notably, *EIF5A* and *DHPS* expression is highly elevated in MYC-overexpressing Burkitt lymphoma (BL; Supplementary Fig. S1D). Indeed, when compared with normal human B-cell subtypes, *EIF5A* is the second most significantly upregulated gene in BL (Supplementary Fig. S1E). Further, IHC analyses of BL and double-hit lymphoma (DHL) patients who bear *MYC* translocations (Moffitt Cancer Center) revealed elevated expression of MYC, eIF5A, and hypusinated eIF5A (eIF5A^{Hyp}) relative to levels expressed in normal lymph nodes (Fig. 1E and F; Supplementary Table S1).

The control of the hypusine circuit by MYC was evaluated using the p493-6 human B lymphoma cell line that harbors a tetracycline-repressible *MYC* transgene (31). Given *EIF5A* is overexpressed across many cancer types (Fig. 1C), it is evident that eIF5A is not regulated solely by MYC. In accord with this, eIF5A protein is expressed at basal levels even in the MYC-off state; however, MYC induction leads to significant increases in the levels of *EIF5A*, *DHPS*, and *DOHH* transcripts, and to increases in the expression of genes encoding the polyamine biosynthetic enzymes, *ODC1*, *AMD1*, *SRM*, and *SMS* (Fig. 1G). Finally, induction of MYC also leads to increases in the levels of DHPS and DOHH proteins (Fig. 1H).

Marked upregulation of the polyamine–hypusine circuit is also manifest in B220$^+$ B cells isolated from the bone marrow (BM) and spleens of Eμ-*Myc* transgenic mice as well as in the lymphomas that arise in these mice (Fig. 1I and J). Furthermore, the hypusinated form of eIF5A (eIF5A^{Hyp}) is substantially elevated in BM premalignant and neoplastic Eμ-*Myc* B cells versus BM B cells from wild-type (WT) littermates (Fig. 1K). Thus, activation of the hypusine circuit is a hallmark of cancer and is especially elevated in MYC-driven lymphoma.

Hypusinated eIF5A Is Essential for Proliferation of MYC-Driven B-cell Lymphoma

The spermidine analogue GC7 (N1-guanyl-1,7-diamineoheptane) competitively inhibits DHPS enzymatic activity (32) and, as expected, GC7 treatment of Eμ-*Myc* B lymphoma cells reduced levels of hypusinated eIF5A (Supplementary Fig. S2A). Moreover, in agreement with other studies (22), low concentrations of GC7 (5–20 μmol/L) effectively inhibited the growth of human Raji BL and mouse Eμ-*Myc* B lymphoma cells (Fig. 2A; Supplementary Fig. S2B), and this response was rescued by the addition of the polyamines putrescine (Put) or spermidine (Spd; Fig. 2B; Supplementary Fig. S2B). However, as previously noted (33), this spermidine analogue may affect other polyamine-engaged pathways independent of the hypusine axis.

Figure 1. Activation of the polyamine–hypusine circuit is a hallmark of MYC-driven cancers. **A,** Schematic of the polyamine–hypusine pathway. AMD1, adenosylmethionine decarboxylase-1; dcSAM, decarboxy SAM; DHPS, deoxyhypusine hydroxylase; DOHH, deoxyhypusine hydroxylase; DFMO, difluoromethylornithine; eIF5A, eukaryotic translation initiation factor 5A; GC7, N1-guanyl-1, 7-diamine-heptane; Hyp, hypusine; ODC, ornithine decarboxylase; SAM, *S*-adenosylmethionine; SMS, spermine synthase; SRM, spermidine synthase. **B,** Copy-number alterations (CNA) of *EIF5A* across different cancer types. The abbreviations for the tumor types are provided in Supplementary Fig. S1A. **C,** *EIF5A* and *EIF5A2* levels in RNA sequencing datasets in 17 cancer types derived from TCGA PanCanAtlas. **D,** *EIF5A* transcript levels relative to normal tissue, classified based on *EIF5A* copy number (TCGA data sets). **E,** Representative hematoxylin and eosin (H&E) staining and IHC of MYC, eIF5A, and hypusinated eIF5A (eIF5A^{Hyp}) proteins in patients with either BL ($n = 7$) or DHL ($n = 18$), or reactive lymph node samples ($n = 13$; Moffitt Cancer Center; scale bar, 50 μm). **F,** Box plots showing IHC staining (%) of the indicated proteins for each patient (open circle). **G,** Expression of genes in the polyamine–hypusine circuit following induction of *MYC* in p493-6 human B-lymphoma cells, as analyzed by qRT-PCR ($n = 3$, fold change to expression at time 0). **H,** Immunoblot analyses of MYC, DHPS, DOHH, eIF5A, and eIF5A^{Hyp} levels in p493-6 human B-lymphoma cells following MYC induction. **I** and **J,** Gene-expression profiling of arrays showing the polyamine-hypusine genes in mouse splenic B220$^+$ B cells from premalignant Eμ-*Myc* ($n = 5$) and wild-type (WT; $n = 4$) mice and Eμ-*Myc* lymphomas ($n = 13$) from GSE32239 (**I**), and bone marrow (BM) of premalignant Eμ-*Myc* ($n = 2$) and WT ($n = 2$) littermate mice from GSE33474 (**J**). Rows represent different probe sets. **K,** Representative immunoblots of eIF5A and eIF5A^{Hyp} in mouse B220$^+$ B cells isolated from BM of 6-week-old WT mice ($n = 5$) and premalignant Eμ-*Myc* mice ($n = 4$), and in lymphomas isolated from Eμ-*Myc* mice ($n = 5$). Levels of significance determined by Mann–Whitney test (**B**), Dunnett multiple comparison (**F**) or unpaired *t* tests (**J**) are indicated as follows: *, $P < 0.05$; **, $P < 0.01$; ***, $P < 0.001$; ****, $P < 0.0001$.

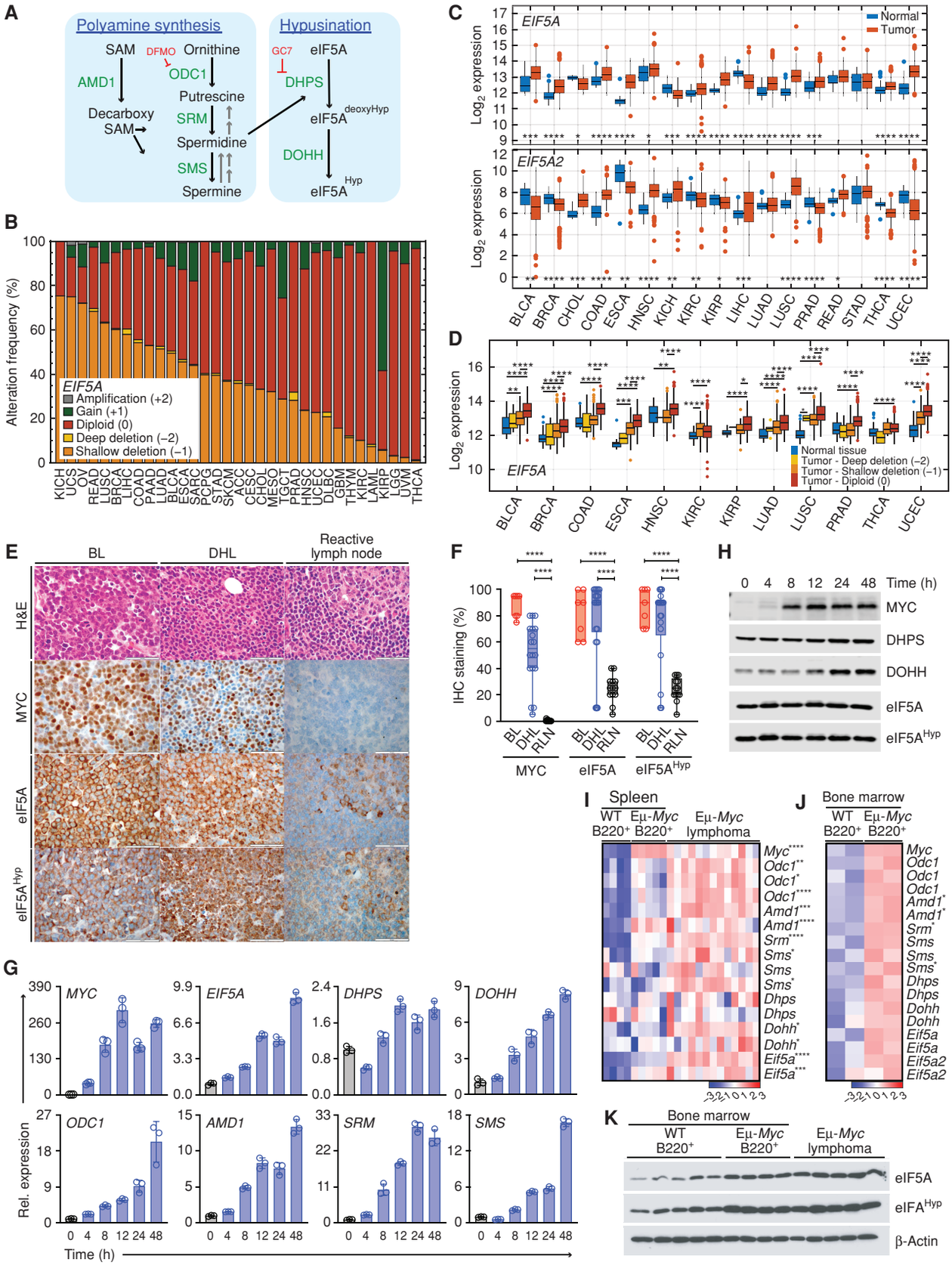
A
Polyamine synthesis
Hypusination
SAM
DFMO
Ornithine
ODC1
AMD1
Putrescine
Decarboxy SAM
SRM
Spermidine
SMS
Spermine
GC7
eIF5A
DHPS
eIF5A deoxyHyp
DOHH
eIF5A Hyp
B
Alteration frequency (%)
EIF5A
Amplification (+2)
Gain (+1)
Diploid (0)
Deep deletion (–2)
Shallow deletion (–1)
KICH UCS OV READ LUSC BRCA LIHC COAD PAAD LUAD BLCA ESCA SARC PCPG STAD SKCM ACC CESC CHOL MESO TGCT PRAD HNSC UCEC DLBC GBM THYM KIRC LAML KIRP LGG UVM THCA
C
EIF5A
EIF5A2
Log2 expression
Normal
Tumor
BLCA BRCA CHOL COAD ESCA HNSC KICH KIRC KIRP LIHC LUAD LUSC PRAD READ STAD THCA UCEC
D
Log2 expression
EIF5A
Normal tissue
Tumor - Deep deletion (–2)
Tumor - Shallow deletion (–1)
Tumor - Diploid (0)
BLCA BRCA COAD ESCA HNSC KIRC KIRP LUAD LUSC PRAD THCA UCEC
E
BL
DHL
Reactive lymph node
H&E
MYC
eIF5A
eIF5A Hyp
F
IHC staining (%)
BL DHL RLN
MYC
eIF5A
eIF5A Hyp
H
0 4 8 12 24 48 Time (h)
MYC
DHPS
DOHH
eIF5A
eIF5A Hyp
I
Spleen
WT B220+
Eμ-Myc B220+
Eμ-Myc lymphoma
Myc Odc1 Amd1 Srm Sms Dhps Dohh Eif5a
J
Bone marrow
WT B220+
Eμ-Myc B220+
Myc Odc1 Amd1 Srm Sms Dhps Dohh Eif5a Eif5a2
G
MYC
EIF5A
DHPS
DOHH
ODC1
AMD1
SRM
SMS
Rel. expression
0 4 8 12 24 48
Time (h)
K
Bone marrow
WT B220+
Eμ-Myc B220+
Eμ-Myc lymphoma
eIF5A
eIFA Hyp
β-Actin

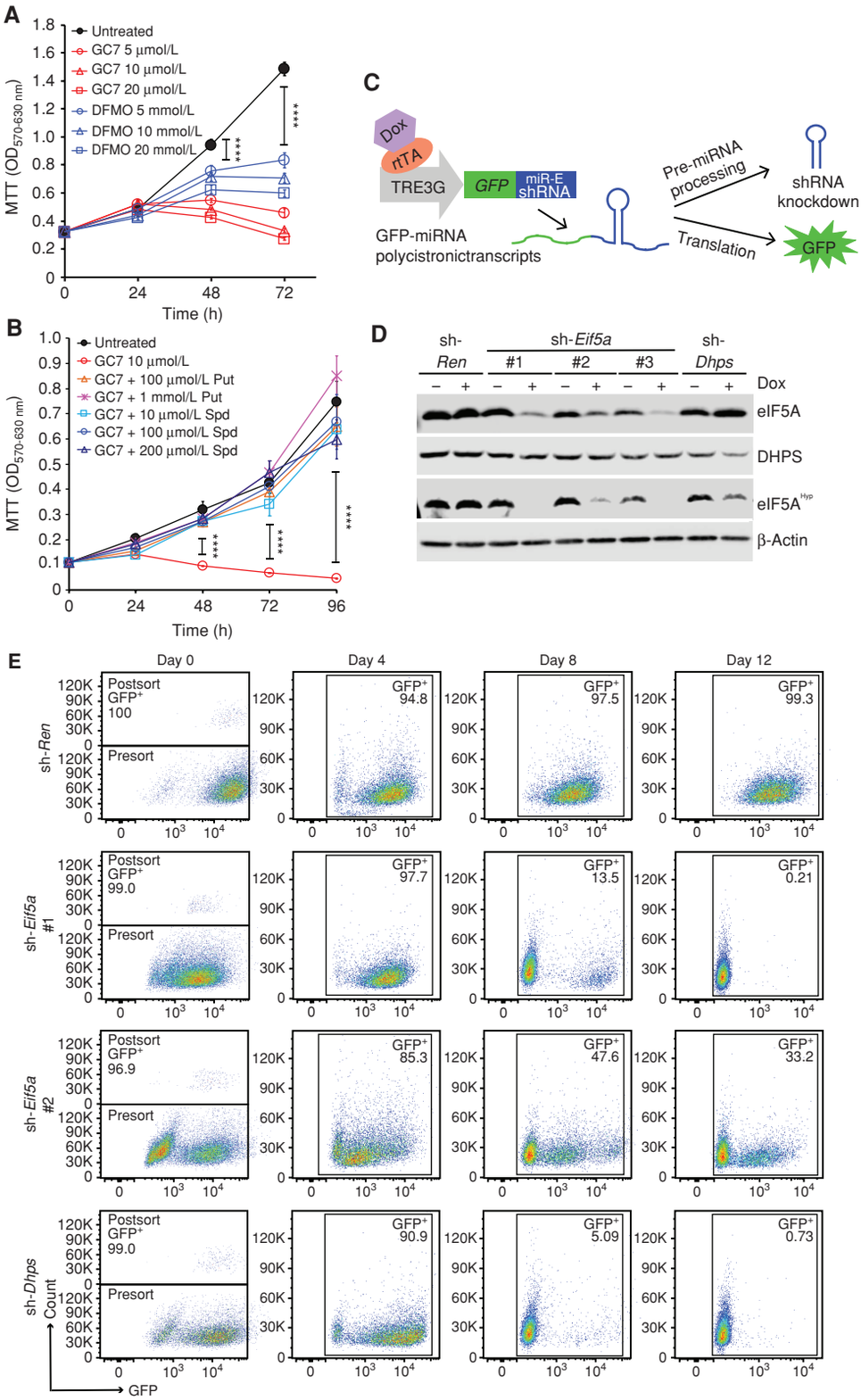

Figure 2. Depletion of eIF5A or DHPS suppresses the growth of human and mouse MYC-driven lymphoma. **A** and **B,** MTT assays showing growth inhibition of human Raji BL cells following treatment with GC7 or DFMO (**A**) and rescue of GC7-induced growth inhibition by addition of putrescine (Put) or spermidine (Spd; $n = 4$; **B**). **C,** Schematic illustrating the miRE shRNA system, which generates *GFP*-shRNA polycistronic transcripts. **D,** Immunoblots showing levels of indicated proteins in Eμ-*Myc*;Rosa26-*rtTA* cells inducibly expressing sh-*Eif5a* #1, sh-*Eif5a* #2, sh-*Eif5a* #3, sh-*Dhps*, or sh-*Ren*. **E,** Representative FACS profile showing retention of cells expressing indicated GFP-shRNAs following cell sort. (*continued on following page*)

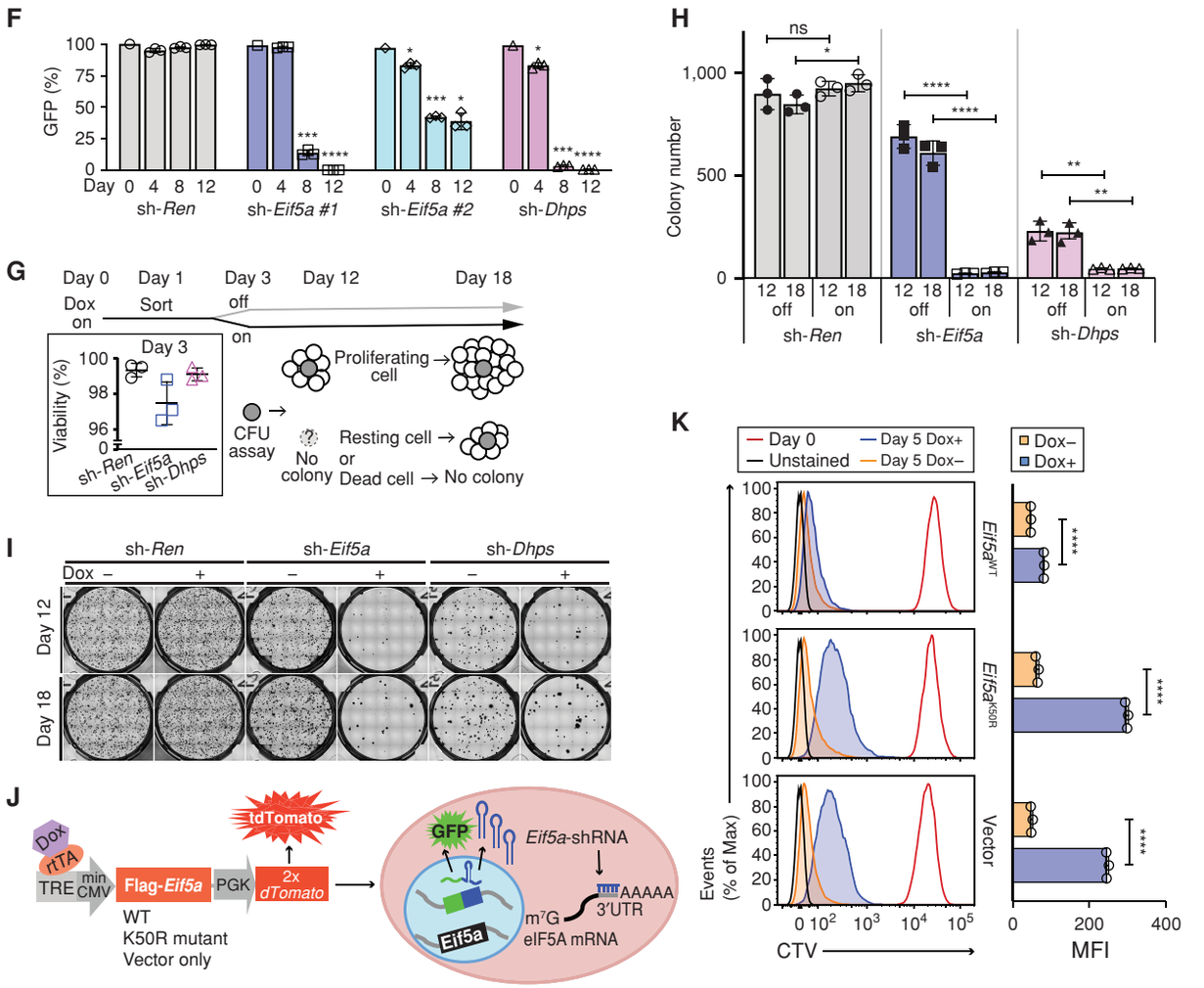

Figure 2. ***(Continued)*** **F,** Quantification of GFP⁺ cell populations at the indicated intervals based on results in **E** ($n = 3$). **G–I,** Methycellulose colony formation unit (CFU) assays evaluating long-term effects of depletion of eIF5A or DHPS on clonogenic potential. **G,** Schematic illustrating the experimental design; inset shows the viability of cells at day 3 as evaluated by trypan blue dye exclusion. **H** and **I,** Representative photos taken at days 12 and 18 showing colony size and number (**H**) and quantification of colony numbers (**I**; $n = 3$). **J,** Schematic of experimental design where sh-*Eif5a*-expressing cells also inducibly express either eIF5A^{WT} or eIF5A^{K50R} or the vector alone. **K,** Rescue of cell proliferation by induction of eIF5A^{WT} in eIF5A-depleted cells, as determined by flow cytometry of CellTrace Violet (CTV) stained cells, and quantification of mean fluorescence intensity (MFI). Left, representative histograms; right, the quantified data of day 5 Dox+ (GFP⁺TdTomato⁺, blue) *vs.* Dox– cells (orange; $n = 3$). Levels of significance determined by unpaired *t* tests are indicated as follows: ns, not significant; *, $P < 0.05$; **, $P < 0.01$; ***, $P < 0.001$; ****, $P < 0.0001$. Error bar indicates mean ± SD. Max, maximum.

To directly examine the effects of loss of function of the hypusine axis, mouse lymphoma lines were derived from Eμ-*Myc*;Rosa26-rt*TA*[2] tumors that express the reverse tetracycline transactivator rtTA[2], and that were engineered to inducibly express short hairpin RNAs (shRNA) targeting *Eif5a*, using a doxycycline (Dox)-regulated system. Dox treatment provoked efficient *Eif5a* knockdown (Supplementary Fig. S2C) and impaired lymphoma cell growth (Supplementary Fig. S2D and S2E).

To precisely track the effects of silencing *Eif5a* or *Dhps*, we also generated Eμ-*Myc*;Rosa26-rt*TA*[2] lymphoma cell lines that inducibly express *GFP*-shRNA polycistronic transcripts (Fig. 2C; ref. 34) and that effectively depleted eIF5A and DHPS proteins following Dox treatment, as well as levels of eIF5A^{Hyp} (Fig. 2D). These cells were then followed for GFP expression to monitor the retention (expression) of the shRNAs by flow cytometry. There was a remarkable selection against the growth of *Eif5a* or *Dhps* shRNA-expressing cells, but not against cells expressing a control shRNA targeting *Renilla luciferase* (sh-*Ren*), which maintained nearly 100% GFP-expressing cells (Fig. 2E and F); thus, *Eif5a* and *Dhps* expression is necessary for lymphoma cell growth. Finally, this response correlated with the efficiency of depletion of eIF5A protein, where lymphoma cells expressing sh-*Eif5a*$_{\#1}$ that was more efficient at knockdown had a more profound phenotype than lymphoma cells expressing the less efficient sh-*Eif5a*$_{\#2}$ (Fig. 2D and E).

Although the half-life of eIF5A protein is very long (>24 hours; ref. 35), tracking cell division with a tracing dye revealed that inhibition of cell proliferation in *Eif5A*- or

Dhps-shRNA expressing cells was first evident 3 days after Dox treatment (Supplementary Fig. S2F). To assess the fate of *Eif5A*- or *Dhps*-shRNA expressing lymphoma cells, these Dox-induced knockdown cell lines (day 0) were sorted for GFP$^+$ at day 1 and cultured in Dox-containing media (Fig. 2G). By day 3, there were no apparent effects on cell viability (Fig. 2G, inset), and an equal number of these cells cultured in Dox media were then plated in methocult media in either the presence or absence of Dox, and colony formation was monitored over time (days 12 and 18). When Dox was removed on day 3, a substantial number of DHPS- or eIF5A-depleted cells were still capable of forming colonies, indicating recovery from knockdown. In contrast, most eIF5A- or DHPS-depleted cells failed to form colonies when kept on Dox over time (day 12), and no newly formed colonies were detected by day 18 of culture (Fig. 2H and I; Supplementary Fig. S2G).

To test if eIF5A hypusination is specifically required for lymphoma cell proliferation, cells expressing *Eif5a*-shRNA that targets the 3′ untranslated region of *Eif5a* mRNA were engineered to also inducibly express comparable levels of FLAG-tagged WT eIF5A or mutant (K50R) eIF5A that cannot be hypusinated (or the vector control, Fig. 2J; Supplementary Fig. S2H). Importantly, forced expression of WT eIF5A, but not the eIF5A-K50R mutant, restored the proliferation of lymphoma cells depleted of endogenous eIF5A (Fig. 2K); thus, eIF5a^{Hyp} is necessary for lymphoma cell proliferation.

eIF5A Hypusination Contributes to Tumorigenic Potential of MYC-Driven Lymphoma

To examine the roles of the hypusine circuit on the tumorigenic potential of MYC-driven lymphoma, we tested the effects of eIF5A depletion in recipient mice bearing Eμ-*Myc*;Rosa26-rt*TA*^{2} lymphomas expressing *Eif5a* shRNA or the control *Renilla* shRNA. On day 3 following transplant, recipient mice were switched to Dox chow or kept on normal chow and were monitored daily (Fig. 3A). These lymphoma cells harbor E255K mutant p53, a DNA binding domain IV mutant whose equivalent site in human *TP53*, E258 (Supplementary Fig. S3A), is a recurrent hotspot in human cancer as revealed by cBioPortal analysis (36). Regardless, selective silencing of *Eif5a*, but not of *Renilla*, impaired lymphomagenic potential (Fig. 3B). Further, analyses of tumors at the endpoint in mice given the Dox-diet revealed that these lymphomas no longer expressed sh-*Eif5a* and reexpressed eIF5A, indicating a selection for tumor cells that escape silencing by the *Eif5a* shRNA (Supplementary Fig. S3B).

These findings were confirmed in pharmacologic studies, where GC7 treatment of Eμ-*Myc* lymphoma reduced eIF5A^{Hyp} levels (Supplementary Fig. S2A) and where GC7 treatment (4 or 20 mg/kg, daily i.p.) of mice transplanted with Eμ-*Myc* lymphoma significantly extended overall survival versus vehicle-treated mice, which rapidly succumbed to disease (Fig. 3C and D; Supplementary Fig. S3C and S3D). Indeed, GC7 treatment was more effective at impairing tumorigenic potential than the clinically used suicide inhibitor of ornithine decarboxylase, DFMO (given in drinking water 1% wt/v; Fig. 3D; Supplementary Fig. S3C and S3D). Thus, eIF5A^{Hyp} contributes to the tumorigenic potential of MYC-driven lymphoma.

Dhps Is Necessary for the Maintenance of MYC-Driven Lymphoma

Given these findings, we reasoned that eIF5A hypusination would be necessary for the maintenance of MYC-driven lymphoma. To establish a system where complete loss of hypusination is achievable, we used the *Dhps*$^{fl/fl}$ conditional knockout mouse model (37), which we crossed to Eμ-*Myc* and Rosa26-*CreER*^{T2} (38) transgenic mice to generate Eμ-*Myc*;Rosa26-*CreER*^{T2};*Dhps*$^{fl/fl}$ and Eμ-*Myc*;Rosa26-*CreER*^{T2};*Dhps*$^{+/+}$ mice. Lymphomas arising in these mice were then harvested (Fig. 3E) and lymphoma cell lines were derived in which the floxed *Dhps* alleles can be deleted by *ex vivo* treatment with 4-hydroxytamoxifen (4-OHT) that activates Cre recombinase. Efficient deletion of the *Dhps* gene and loss of DHPS protein were confirmed by genomic PCR and immunoblot analyses (Supplementary Fig. S3E and S3F). Loss of DHPS protein led to marked reductions in levels of eIF5A^{Hyp} without affecting the total levels of eIF5A (Fig. 3F). Further, consistent with reduced clonogenic survival potential observed following shRNA silencing of *Dhps* or *Eif5a* (Fig. 2I; Supplementary Fig. S2G), Cre-directed loss of *Dhps*, and as a consequence loss of eIF5A^{Hyp}, ultimately led to cell death (Fig. 3G).

To assess the role of Dhps in tumor maintenance, Eμ-*Myc*;Rosa26-*CreER*^{T2};*Dhps*$^{fl/fl}$ and Eμ-*Myc*;Rosa26-*CreER*^{T2};*Dhps*$^{+/+}$ lymphoma cells engineered to express the bioluminescence reporter OgNLuc+ were injected subcutaneously into Nude mice and tumor growth was monitored daily by measurement of tumor volumes and twice a week by bioluminescence imaging (BLI; Fig. 3E and H–J). Once tumors were palpable, mice were randomized to vehicle or tamoxifen cohorts and were treated for 9 consecutive days. Importantly, *Dhps* loss significantly impaired tumor progression

Figure 3. Hypusinated eIF5A is necessary for the growth and maintenance of Myc-driven lymphoma. **A,** Experimental design of lymphoma transplant studies; **B,** Kaplan–Meier survival curves of mice transplanted i.v. with Eμ-*Myc*;Rosa26-rt*TA*^{2} lymphoma cells that inducibly express sh-*Eif5a* or sh-*Ren*. Median survival of cohorts: sh-*Ren* Dox– 21 days; sh-*Ren* Dox+ 20.5 days; sh-*Eif5a* Dox– 21.5 days; and sh-*Eif5a* Dox+ 29 days. **C** and **D,** Experimental design of Eμ-*Myc* lymphoma transplant studies testing the efficacy of DFMO (1% wt/vol, in drinking water) and GC7 (20 mg/kg, daily i.p.; **C**) versus vehicle and Kaplan–Meier survival curves of treated mice (**D**; vehicle, median survival 15 days; DFMO, median survival 22 days; GC7, median survival 26 days). DFMO- and GC7-treated mice showed no obvious toxicities. **E,** Experimental design of subcutaneous (sub-Q) transplant studies of lymphoma cells established from tumors of Eμ-*Myc*;*CreER*^{T2};*Dhps*$^{fl/fl}$ or Eμ-*Myc*;*CreER*^{T2};*Dhps*$^{+/+}$ mice. **F,** Immunoblots showing levels of indicated proteins in Eμ-*Myc*;*Cre-ER*^{T2};*Dhps*$^{fl/fl}$ or Eμ-*Myc*;*Cre-ER*^{T2};*Dhps*$^{+/+}$ lymphoma cells following treatment with 4-OHT. **G,** Left, representative FACS profiles showing apoptosis upon loss of *Dhps* as analyzed by Annexin V–FITC/PI labeling; right, quantification ($n = 3$). **H,** Lymphoma growth in transplanted mice following treatment with vehicle (corn oil) or TAM (tamoxifen). Blue arrowhead indicates the average tumor volume at the start of the TAM treatment: 21 mm^3 (Vehicle group: 18 mm^3). Black arrowheads indicate dates when treatment was started (day 0) and terminated (day 9; $n = 13$). **I,** Total flux analyzed by BLI of the same mice bearing Eμ-*Myc*;*Cre-ER*^{T2};*Dhps*$^{fl/fl}$ lymphomas ($n = 13$). **J,** Representative BLI of mice that were treated with TAM or vehicle. Days after treatment start are indicated (white inset). Levels of significance determined by Mantel–Cox log-rank test (**B**) and (**D**), or unpaired *t* tests (**G**) are indicated as follows: *, $P < 0.05$; **, $P < 0.01$; ***, $P < 0.001$; ****, $P < 0.0001$. Error bar, mean ± SD (**G**) or mean ± SEM (**H**) and (**I**).

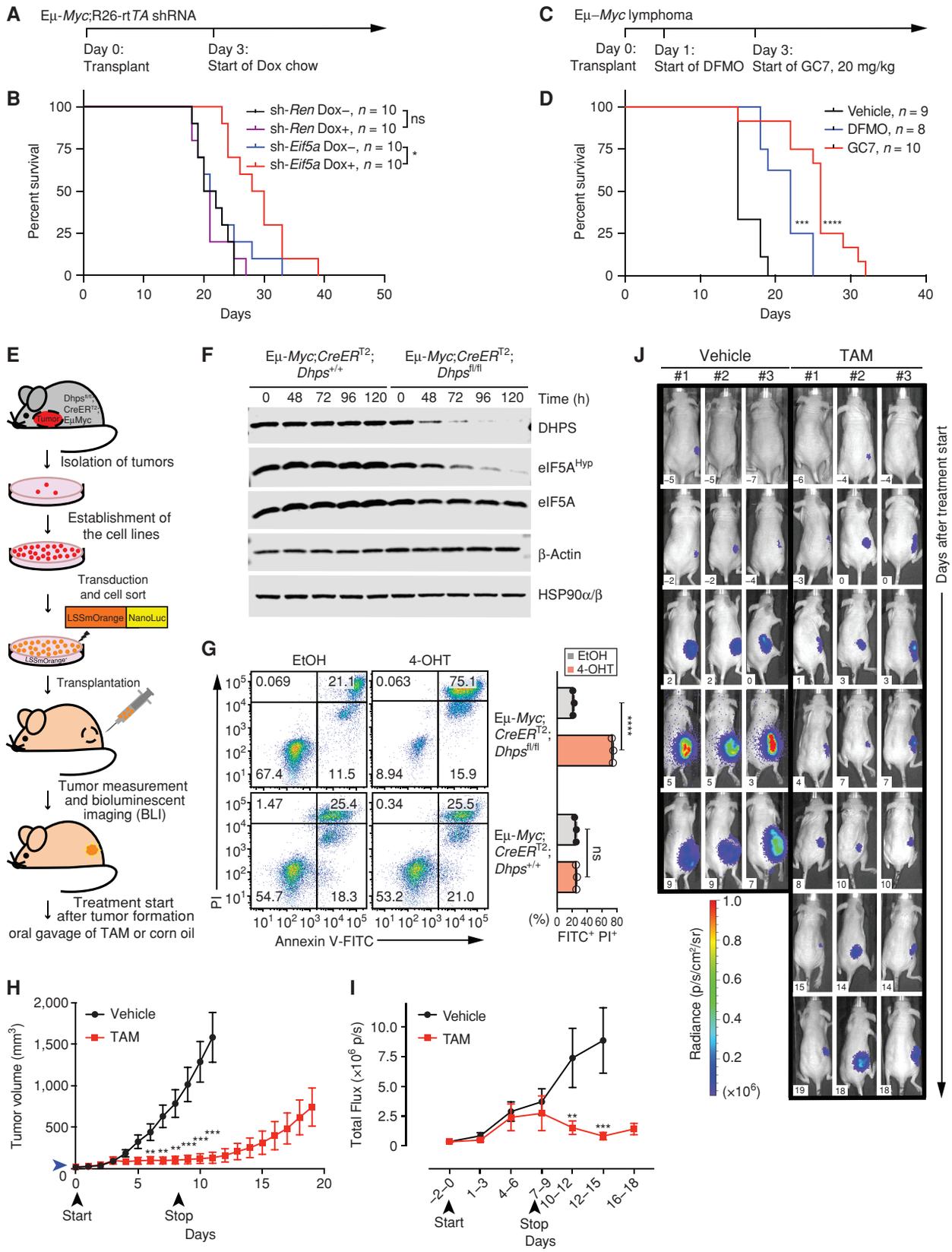
A
Eμ-Myc;R26-rtTA shRNA
Day 0: Transplant
Day 3: Start of Dox chow
B
Percent survival
Days
sh-Ren Dox–, n = 10
sh-Ren Dox+, n = 10
sh-Eif5a Dox–, n = 10
sh-Eif5a Dox+, n = 10
ns
*
C
Eμ–Myc lymphoma
Day 0: Transplant
Day 1: Start of DFMO
Day 3: Start of GC7, 20 mg/kg
D
Percent survival
Days
Vehicle, n = 9
DFMO, n = 8
GC7, n = 10
***
****
E
Isolation of tumors
Establishment of the cell lines
Transduction and cell sort
LSSmOrange
NanoLuc
Transplantation
Tumor measurement and bioluminescent imaging (BLI)
Treatment start after tumor formation
oral gavage of TAM or corn oil
F
Eμ-Myc;CreER^T2; Dhps^+/+
Eμ-Myc;CreER^T2; Dhps^fl/fl
Time (h)
DHPS
eIF5A^Hyp
eIF5A
β-Actin
HSP90α/β
G
EtOH
4-OHT
PI
Annexin V-FITC
Eμ-Myc; CreER^T2; Dhps^fl/fl
Eμ-Myc; CreER^T2; Dhps^+/+
****
ns
FITC+ PI+
J
Vehicle
TAM
Days after treatment start
Radiance (p/s/cm²/sr)
(×10^6)
H
Tumor volume (mm³)
Vehicle
TAM
Start
Stop
Days
I
Total Flux (×10^6 p/s)
Vehicle
TAM
Start
Stop
Days

(Fig. 3H–J), whereas lymphoma growth continued unabated in vehicle-treated mice (Supplementary Fig. S3G). Remarkably, 5 out of 13 tamoxifen-treated mice bearing Eμ-*Myc*;Rosa26-*CreER*^{T2};*Dhps*$^{fl/fl}$ lymphomas displayed nearly complete tumor regression. Nonetheless, once tamoxifen treatment was terminated (at day 9), following a lag period all tumors started to regrow (Fig. 3H), and these mice reexpressed DHPS (Supplementary Fig. S3H). Thus, there is a strong selection against loss of the hypusine circuit in the maintenance of MYC-driven lymphoma.

Depletion of eIF5A or DHPS Disrupts Select MYC-Dependent Transcription Programs

Hypusinated eIF5A likely affects diverse cellular pathways, for example, through direct regulation of its translational targets or via secondary effects on other biological processes (Fig. 4A). Therefore, we examined the global effects of knockdown of *Eif5a* and *Dhps* on the transcriptome, proteome, and translational landscape of MYC-induced lymphoma. For these studies, we used Eμ-*Myc*;Rosa26-rt*TA*^{2} lymphoma cells depleted of eIF5A or DHPS for 72 hours, an interval where the cells were still viable (Fig. 2G, inset). RNA sequencing (RNA-seq) revealed 2,450 differentially expressed genes (DEG) in *Eif5a*-depleted lymphoma cells, and 1,286 DEGs in *Dhps*-knockdown cells relative to control cells (sh-*Ren*). No DEGs were detected in control sh-*Ren* cells treated with and without Dox; thus, there are minimal effects of Dox on gene expression in this model (Supplementary Fig. S4A). Further, 383 significantly upregulated and 333 significantly downregulated genes were shared between *Eif5a*- and *Dhps*-depleted cells (Fig. 4B). Among these shared genes, Metascape gene set enrichment analysis (39) showed that ribosome biogenesis, B-cell regulation/activation, and the immune response are the major enriched functional categories represented by upregulated genes (Fig. 4C; Supplementary Fig. S4B), whereas enriched functional terms for shared downregulated genes include diverse central cellular processes, including cell division (Supplementary Fig. S4C). Further, genes in the polyamine–hypusine circuit, including the direct MYC transcription targets *Odc1* and *Srm1*, were also upregulated (Supplementary Fig. S4D); thus, the initial cellular response to inhibiting the hypusine circuit includes a compensatory upregulation of this pathway.

Next, we assessed how the depletion of eIF5A or Dhps affects MYC-controlled transcription programs. Previous studies established 1,941 MYC-dysregulated genes ($q < 0.05$) in Eμ-*Myc* lymphomas (40), and that upregulated genes represent pathways involved in the control of the cell cycle, ribosome biogenesis, and metabolism (Fig. 4D). In contrast, MYC-downregulated genes represent pathways controlling the immune response, and B-cell regulation/activation (ref. 40; Fig. 4D). Integrating our RNA-seq data with MYC-dysregulated genes (Fig. 4E) revealed that eIF5A or DHPS depletion has two major effects on MYC-regulated pathways. First, immune regulatory genes that are significantly downregulated in Eμ-*Myc* lymphoma are actually increased or reexpressed following silencing of *Eif5a* or *Dhps* (Fig. 4F; Supplementary Table S2). Interestingly, such immune genes encode cell-surface proteins such as CD19 that are targets for antibody and chimeric antigen receptor (CAR) T therapy, and that are occasionally silenced in treatment-naïve lymphoma and are often silenced in patients who fail CD19-targeted therapies (41, 42). Specifically, the Eμ-*Myc*;Rosa26-rt*TA*^{2} lymphoma line used in our studies is unusual in that it does not express several B-cell-specific receptors including CD19 and, quite strikingly, *CD19* expression, as well as that of several other B cell–specific receptors (e.g., *CD79a* and *CD79b*), are induced following depletion of eIF5A or DHPS (Fig. 4G).

Second, expression of 20% and 10% of the 1,236 MYC-upregulated genes manifest in Eμ-Myc lymphoma was significantly altered following eIF5A or DHPS depletion (sh-*Eif5a*, 229; sh-*Dhps*, 132; 81 common genes, $q < 0.05$), respectively (Fig. 4F). Among these altered genes, the downregulated genes are enriched for cell-cycle control genes, including several E2F transcription targets (e.g., *Ccne2* and *Bub1*, Fig. 4F; Supplementary Table S2). Thus, the initial proliferation inhibitory phenotype provoked by eIF5A or DHPS depletion (Fig. 2K; Supplementary Fig. S2F) is associated with the suppression of transcription targets that are necessary for cell-cycle progression.

The Hypusine-Dependent Translational Landscape of MYC-Driven Lymphoma

To identify eIF5A^{Hyp}-dependent translation targets that might contribute to lymphoma growth and survival, we determined the global effects of silencing *Eif5a* or *Dhps* on translation by performing ribosome profiling (43) in parallel with RNA-seq. Further, to assess potential effects on steady-state protein levels, tandem mass tag (TMT)-multilabeling mass spectrometry (44) was performed following *Eif5a* or *Dhps* knockdown. Translation efficiency (TE) was then determined as the ratio of the levels of ribosome-bound mRNAs (those being actively translated) to mRNA levels for each gene (45). Reproducibility for each transcript analyzed (RNA-seq, TE) was validated in biological duplicates of sh-*Ren*-, sh-*Eif5a*-, and sh-*Dhps*-expressing lymphoma cells (Supplementary Fig. S5A). Further, the 10-plex TMT proteomics time-course analyses identified over 6,400 proteins

Figure 4. The hypusine circuit controls select transcriptional networks manifest in MYC-driven lymphoma. **A,** Schematic of possible direct or indirect effects provoked by silencing *Eif5A* or *Dhps*. **B,** Venn diagram of differentially expressed genes (DEG) in Eμ-*Myc* lymphoma cells following depletion of eIF5A (blue) or DHPS (pink; $q < 0.05$). **C,** Network enrichment analysis by Metascape (39) of the shared 383 genes significantly upregulated following depletion of eIF5A or DHPS in Eμ-*Myc* lymphoma cells. Each cluster is represented by different colors, and a circle node represents each enriched functional term. **D,** Metascape enrichment analysis of significantly up- and downregulated genes in B220$^+$ splenic Eμ-*Myc* lymphoma cells versus WT B220$^+$ splenic B cells (40). Cell-cycle regulation, ribosome biogenesis, and B-cell signaling/activation pathways are indicated in blue, red, and green, respectively, and the dotted line shows $q = 0.05$. **E,** Venn diagram showing overlap of DEGs present in Eμ-*Myc* lymphoma (dotted yellow line) with DEGs of eIF5A- or DHPS-depleted Eμ-*Myc* lymphoma cells (blue or pink, respectively, defined by comparing their expression to *sh-Ren* controls). 141 MYC-deregulated genes were differentially expressed in both eIF5A- and DHPS-depleted Eμ-*Myc* cells. **F,** Heat maps showing changes in mRNA levels manifest in MYC-dysregulated genes in Eμ-*Myc* lymphoma cells that are significantly and commonly altered by eIF5A or DHPS depletion (left), representative genes (middle), and top 5 pathways defined by ontology analysis (right). **G,** Relative $\log_2$ expression of genes of B-cell regulation/activation pathways (e.g., CD19, CD79a, CD79b, shown in red) whose expression is induced following depletion of eIF5A or DHPS. All genes are DEG ($q < 0.05$).

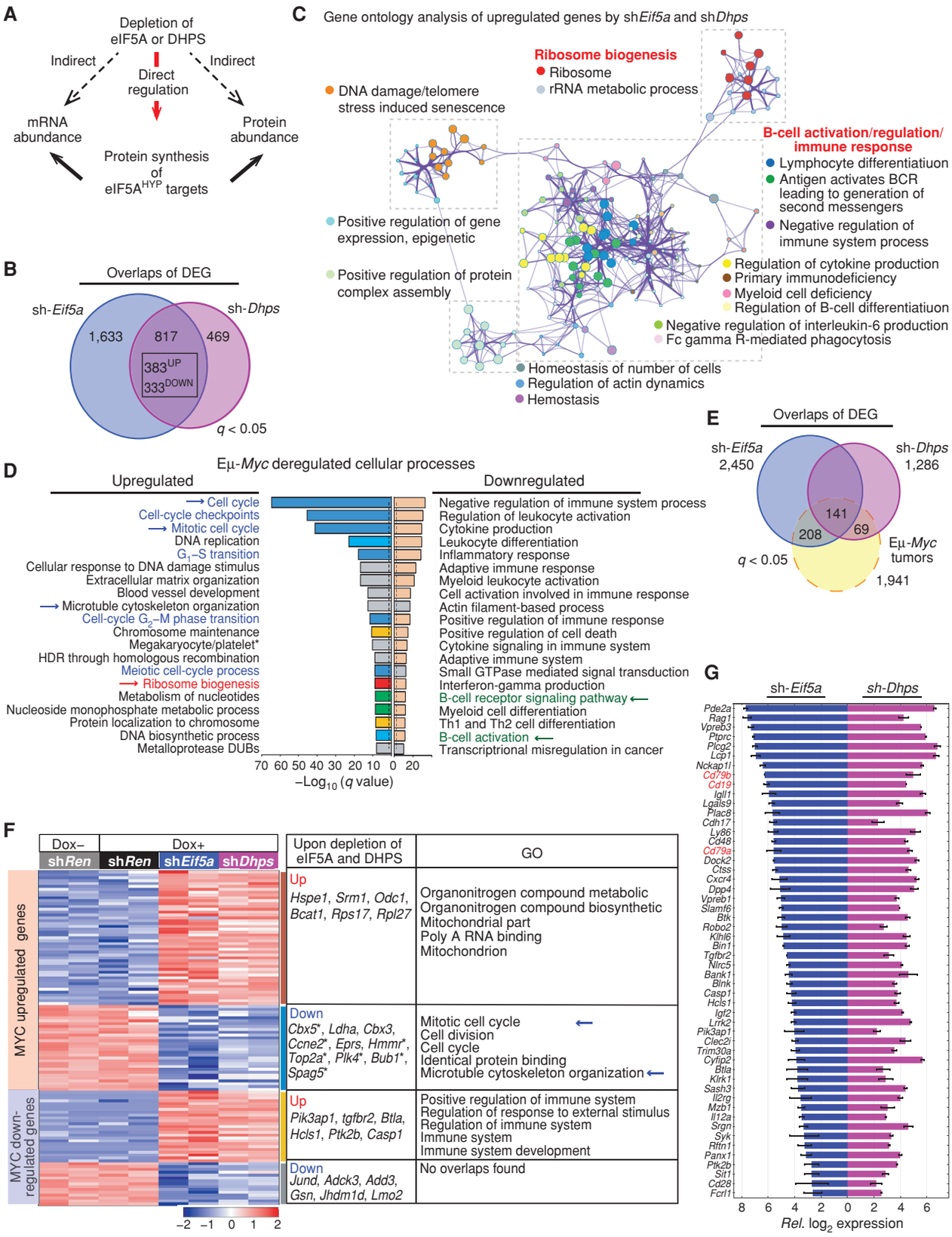
A
Depletion of eIF5A or DHPS
Indirect
Direct regulation
Indirect
mRNA abundance
Protein abundance
Protein synthesis of eIF5A^HYP targets
B
Overlaps of DEG
sh-Eif5a
sh-Dhps
1,633
817
469
383^UP
333^DOWN
q < 0.05
C
Gene ontology analysis of upregulated genes by shEif5a and shDhps
Ribosome biogenesis
Ribosome
rRNA metabolic process
DNA damage/telomere stress induced senescence
B-cell activation/regulation/ immune response
Lymphocyte differentiatiuon
Antigen activates BCR leading to generation of second messengers
Negative regulation of immune system process
Positive regulation of gene expression, epigenetic
Positive regulation of protein complex assembly
Regulation of cytokine production
Primary immunodeficiency
Myeloid cell deficiency
Regulation of B-cell differentiatiuon
Negative regulation of interleukin-6 production
Fc gamma R-mediated phagocytosis
Homeostasis of number of cells
Regulation of actin dynamics
Hemostasis
D
Eμ-Myc deregulated cellular processes
Upregulated
Cell cycle
Cell-cycle checkpoints
Mitotic cell cycle
DNA replication
G1–S transition
Cellular response to DNA damage stimulus
Extracellular matrix organization
Blood vessel development
Microtuble cytoskeleton organization
Cell-cycle G2–M phase transition
Chromosome maintenance
Megakaryocyte/platelet*
HDR through homologous recombination
Meiotic cell-cycle process
Ribosome biogenesis
Metabolism of nucleotides
Nucleoside monophosphate metabolic process
Protein localization to chromosome
DNA biosynthetic process
Metalloprotease DUBs
70 60 50 40 30 20 10 0 20
–Log10 (q value)
Downregulated
Negative regulation of immune system process
Regulation of leukocyte activation
Cytokine production
Leukocyte differentiation
Inflammatory response
Adaptive immune response
Myeloid leukocyte activation
Cell activation involved in immune response
Actin filament-based process
Positive regulation of immune response
Positive regulation of cell death
Cytokine signaling in immune system
Adaptive immune system
Small GTPase mediated signal transduction
Interferon-gamma production
B-cell receptor signaling pathway
Myeloid cell differentiation
Th1 and Th2 cell differentiation
B-cell activation
Transcriptrional misregulation in cancer
E
Overlaps of DEG
sh-Eif5a
2,450
sh-Dhps
1,286
141
208
69
q < 0.05
Eμ-Myc tumors
1,941
F
Dox–
Dox+
shRen
shRen
shEif5a
shDhps
MYC upregulated genes
MYC down-regulated genes
–2 –1 0 1 2
Upon depletion of eIF5A and DHPS
GO
Up
Hspe1, Srm1, Odc1, Bcat1, Rps17, Rpl27
Organonitrogen compound metabolic
Organonitrogen compound biosynthetic
Mitochondrial part
Poly A RNA binding
Mitochondrion
Down
Cbx5*, Ldha, Cbx3, Ccne2*, Eprs, Hmmr*, Top2a*, Plk4*, Bub1*, Spag5*
Mitotic cell cycle
Cell division
Cell cycle
Identical protein binding
Microtuble cytoskeleton organization
Up
Pik3ap1, tgfbr2, Btla, Hcls1, Ptk2b, Casp1
Positive regulation of immune system
Regulation of response to external stimulus
Regulation of immune system
Immune system
Immune system development
Down
Jund, Adck3, Add3, Gsn, Jhdm1d, Lmo2
No overlaps found
G
sh-Eif5a
sh-Dhps
Pde2a
Rag1
Vpreb3
Ptprc
Plcg2
Lcp1
Nckap1l
Cd79b
Cd19
Igll1
Lgals9
Plac8
Cdh17
Ly86
Cd48
Cd79a
Dock2
Ctss
Cxcr4
Dpp4
Vpreb1
Slamf6
Btk
Robo2
Klhl6
Bin1
Tgfbr2
Nlrc5
Bank1
Blnk
Casp1
Hcls1
Igf2
Lrk2
Pik3ap1
Clec2i
Trim30a
Cyfip2
Btla
Klrk1
Sash3
Il2rg
Mzb1
Il12a
Srgn
Syk
Rftn1
Panx1
Ptk2b
Sit1
Cd28
Fcrl1
8 6 4 2 0 2 4 6
Rel. log2 expression

for the sh-*Ren*, sh-*Eif5a*, and sh-*Dhps* cohorts (Supplementary Fig. S5B).

As expected given their functions in the hypusine axis, the directionality of $\log_2$-fold changes resulting from eIF5A depletion versus control sh*Ren* cells was highly concordant with those changes caused by depletion of DHPS in all three parameters: RNA-seq, TE, and steady-state protein levels (Fig. 5A). Furthermore, although there was an expected correlation of RNA-seq and ribosome sequencing (Ribo-seq), there were no overall correlations in TE and RNA-seq (Fig. 5B; Supplementary Fig. S5C). Thus, the changes in mRNA levels and their TE that are observed following depletion of eIF5A or DHPS are largely independent of each other, underscoring the key roles of hypusination in translational control.

To assess the spectrum of lymphoma mRNAs whose translation is dependent on eIF5A or DHPS, global analyses of TE were performed. These analyses identified 665 shared differentially translated transcripts (DTT, $P < 0.05$) in sh-*Eif5a*- or sh-*Dhps*-expressing lymphoma cells (Supplementary Table S3). Importantly, 88% of these DDT had reduced TE (TE^{low}: 584 mRNAs), indicating $eIF5A^{Hyp}$ is indeed necessary for their efficient translation (Fig. 5C). Supporting previous studies showing that eIF5A promotes translation of mRNAs containing sequential polyproline (poly-P) codons (>3; ref. 28), analyses of the number of poly-P motifs within a given mRNA revealed that depletion of eIF5A or DHPS generally reduced the TE of mRNAs having multiple poly-P motifs (Supplementary Fig. S5D). Interestingly, however, the majority of mRNAs having TE^{low} following depletion of eIF5A or DHPS lacked consecutive poly-P codons, indicating that the role of eIF5A in promoting efficient translation is not limited to transcripts containing poly-P codons. Finally, gene enrichment analysis of these hypusine-dependent translation targets revealed that TE^{low} genes has roles in key cellular processes, including regulation of the cell cycle (Fig. 5D).

$eIF5A^{Hyp}$ Controls Oncogenic Translation and Transcription Programs in Lymphoma

Notably, DTTs included a substantial number of genes that have established roles in cancer, including tumor suppressors and oncogenes. Specifically, from 2,579 potential oncogenic drivers and tumor suppressors, we identified 244 (TE^{low}: 173) and 204 (TE^{low}: 176) transcripts whose translation was significantly altered upon depletion of eIF5A or DHPS, respectively (129 shared mRNAs with 113 TE^{low}, 15 TE^{high}, and 1 discordant transcript; Supplementary Table S4). Ranking these DTTs based on fold changes in TE revealed that over 80% of mRNAs encoding potential oncogenic drivers had reduced translation efficiency following the knockdown of eIF5A or DHPS (Fig. 5E). Importantly, these TE^{low} transcripts include genes known to play critical roles in cell growth across different lymphoma subtypes (e.g., *E2f2*, *Pim3*).

Because steady-state levels of proteins are a function of both their synthesis and turnover rates, not all TE^{low} genes identified following the knockdown of *Eif5a* or *Dhps* showed an immediate reduction in their corresponding protein levels. We thus reasoned that TE^{low} genes that contribute to phenotypes provoked by depletion of eIF5A or DHPS encode proteins whose steady-state levels are consistently reduced upon knockdown of *Eif5a* or *Dhps*. To assess this, we performed a time-course TMT proteomic analysis. These studies revealed that several TE^{low} genes have consistent reductions in the levels of their corresponding proteins, including Huntingtin (HTT; Fig. 5F) that is widely known as the protein mutated in a neurologic disorder, Huntington's disease, but is also ubiquitously expressed in many cell types, including B cells (Supplementary Fig. S5E) and WT HTT possesses antiapoptotic function (46). In addition, there were reductions in POLD1 (Fig. 5F), which is the catalytic subunit of DNA polymerase-δ that directs the synthesis of the lagging strand during DNA replication and that, together with DNA polymerase-ε, directs DNA synthesis of over 90% of the genome (47). Interestingly, *POLD1* is overexpressed in many cancer types, unlike *POLD-2*, *-3*, and *-4* genes that encode accessory subunits (Supplementary Fig. S5F). Furthermore, there were reductions in the steady-state levels of the metabolic enzyme Stearoyl-CoA desaturase (SCD1; Fig. 5F), which generates unsaturated lipids required for the maintenance of endoplasmic reticulum (ER) membrane homeostasis and for preventing MYC-mediated ER stress. Notably, SCD1 contributes to the growth and survival of MYC-driven lymphoma (48).

To validate these hypusine targets and to test if changes in their protein levels are associated with loss of hypusination, we evaluated their levels in eIF5A knockdown lymphoma cells that also inducibly express exogenous WT eIF5A or the hypusine-defective $eIF5A^{K50R}$ mutant. In accord with the profound defects in cell proliferation observed following depletion of $eIF5A^{Hyp}$ (Fig. 2K; Supplementary Fig. S2F), immunoblot analyses confirmed that eIF5A depletion provoked reductions in protein levels of several hypusine targets known to contribute to cell-cycle progression, including POLD1, E2F2, PIM3, JUND, and Cyclin D3 (Fig. 6A and B, c.f., lanes 1 vs. lanes 2). Moreover, inducible

Figure 5. The $eIF5A^{Hyp}$-dependent translational landscape of Eμ-*Myc* lymphoma. **A,** Correlation plots showing concordant effects of *Eif5A* and *Dhps* knockdown on gene expression (left, R = 0.738), translation efficiency (middle, TE, R = 0.503), and steady-state protein levels (right, R = 0.624) in sh-*Eif5a*- and sh-*Dhps*- vs. sh-*Ren*-expressing Eμ-*Myc* lymphoma cells. Correlations are displayed as scatterplots where green, blue, and pink colors indicate significance for both sh-*Eif5a*- and sh-*Dhps* (green), for only sh-*Eif5a* (blue), or for only sh-*Dhps* (pink); gray, not significant. Black denotes proteomic samples at the 96 hours time point. $q < 0.05$ was used to determine the significance for RNA-seq and $P < 0.05$ was used for TE data sets. **B,** Scatter plots showing correlation among $\log_2$ fold changes in RNA-seq, Ribo-seq, and TE analyses following eIF5A depletion. Blue indicates differentially translated transcripts (DTT, $P < 0.05$); gray indicates nonsignificant transcripts. **C,** Venn diagram of DTTs in sh-*Eif5a*- (blue) or sh-*Dhps*- (pink) knockdown Eμ-*Myc* lymphoma cells ($P < 0.05$; 657 concordantly shared transcripts, TE^{low}: 584 and TE^{high}: 73). **D,** Metascape enrichment analysis of the 584 TE^{low} genes showing the top 10 categories. The dotted line shows $q = 0.05$. **E,** A ranked list of $\log_2$-fold change of TE for 244 and 204 differentially translated oncogenes (circles) and tumor suppressors (triangles) in eIF5A- (left) or DHPS- (right) depleted cells. Dot colors indicate significance for both sh-*Eif5a* and sh-*Dhps* (green), for only sh-*Eif5a* (blue), or for only sh-*Dhps* (pink). Names of select oncogenes are in black; tumor suppressors are in red. **F,** Identification of shared TE^{low} transcripts having reduced levels of their corresponding proteins following *Eif5a* or *Dhps* knockdown in Eμ-*Myc* lymphoma. Left, heat maps of all transcripts sorted based on low to high TE-$\log_2$ fold changes (green columns 2 and 7). Orange column (columns 1 and 6) indicates RNA-seq $\log_2$ fold changes of these transcripts (72 hours). Yellow columns indicate the time course of TMT proteomic analyses (72, 96, and 120 hours). Right, among the shared significant TE^{low} transcripts ($P < 0.05$), a time-course analysis of concordantly reduced encoded proteins in both sh-*Eif5a* and sh-*Dhps* cells.

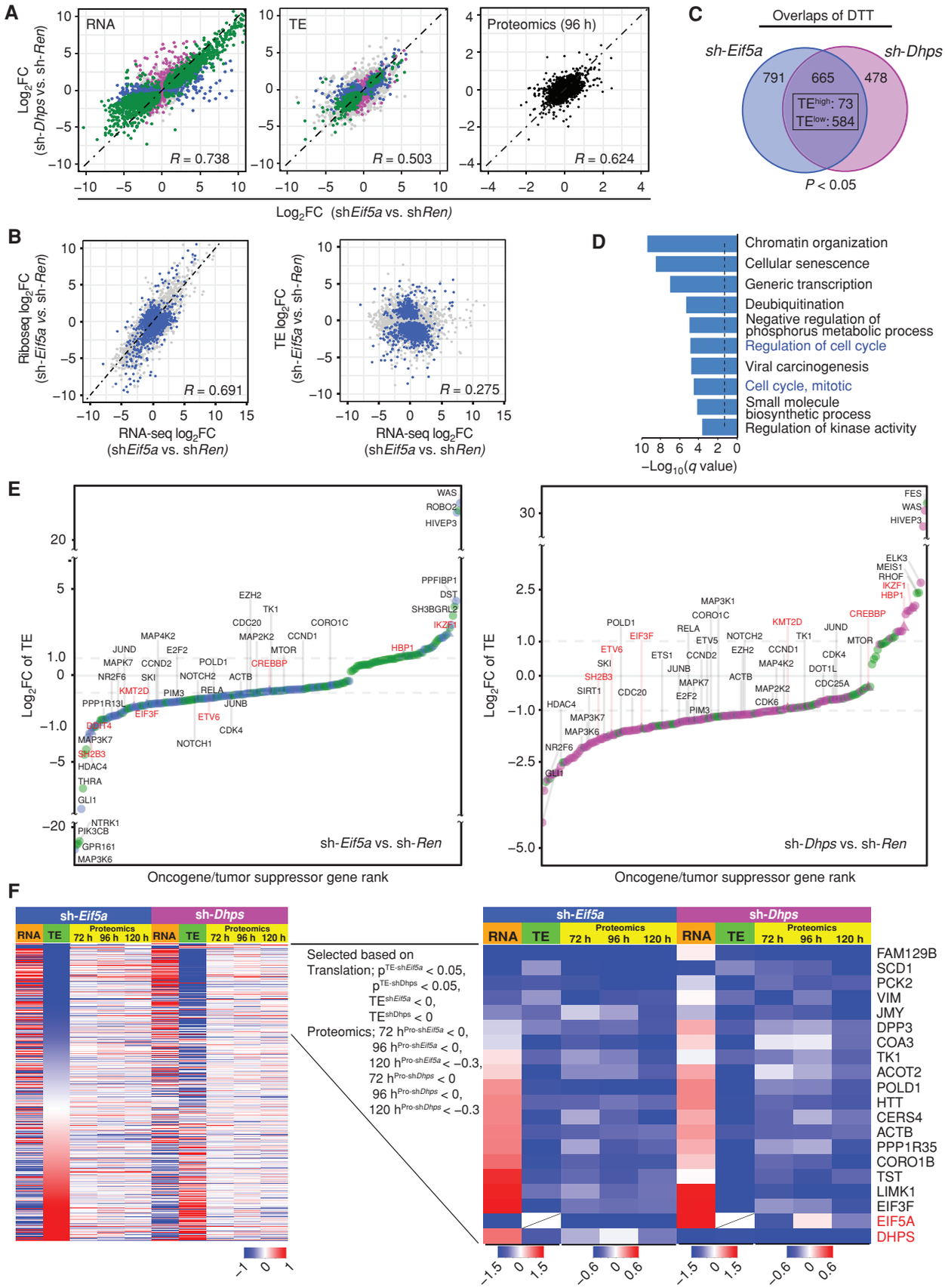
A
RNA
TE
Proteomics (96 h)
R = 0.738
R = 0.503
R = 0.624
Log2FC (sh-Dhps vs. sh-Ren)
Log2FC (shEif5a vs. shRen)
B
Riboseq log2FC (sh-Eif5a vs. sh-Ren)
TE log2FC (sh-Eif5a vs. sh-Ren)
R = 0.691
R = 0.275
RNA-seq log2FC (shEif5a vs. shRen)
C
Overlaps of DTT
sh-Eif5a
sh-Dhps
791
665
478
TEhigh: 73
TElow: 584
P < 0.05
D
Chromatin organization
Cellular senescence
Generic transcription
Deubiquitination
Negative regulation of phosphorus metabolic process
Regulation of cell cycle
Viral carcinogenesis
Cell cycle, mitotic
Small molecule biosynthetic process
Regulation of kinase activity
−Log10(q value)
E
Log2FC of TE
sh-Eif5a vs. sh-Ren
sh-Dhps vs. sh-Ren
Oncogene/tumor suppressor gene rank
F
sh-Eif5a
sh-Dhps
RNA
TE
Proteomics
72 h
96 h
120 h
Selected based on
Translation; pTE-shEif5a < 0.05,
pTE-shDhps < 0.05,
TEshEif5a < 0,
TEshDhps < 0
Proteomics; 72 hPro-shEif5a < 0,
96 hPro-shEif5a < 0,
120 hPro-shEif5a < −0.3,
72 hPro-shDhps < 0
96 hPro-shDhps < 0,
120 hPro-shDhps < −0.3
FAM129B
SCD1
PCK2
VIM
JMY
DPP3
COA3
TK1
ACOT2
POLD1
HTT
CERS4
ACTB
PPP1R35
CORO1B
TST
LIMK1
EIF3F
EIF5A
DHPS

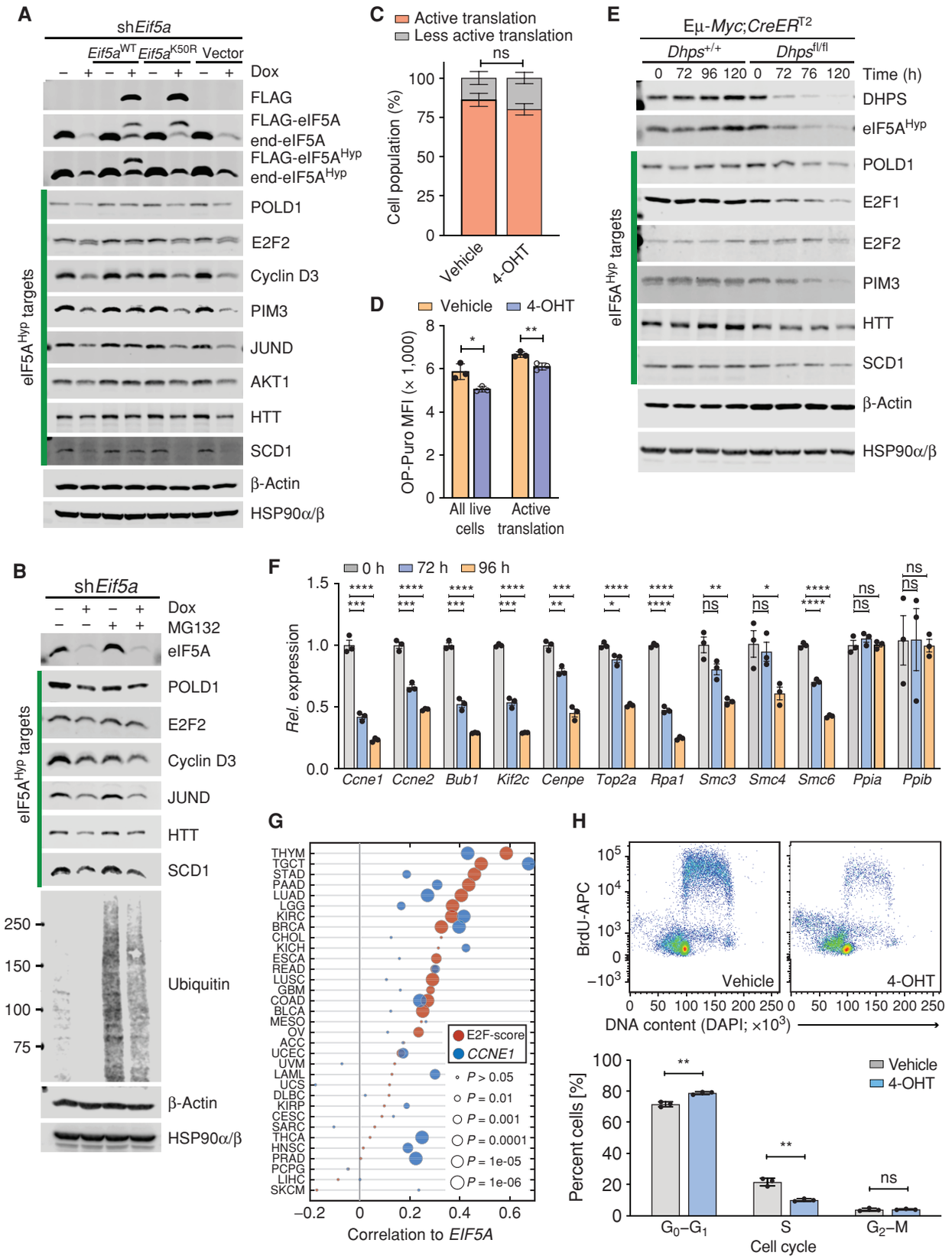
A
shEif5a
Eif5a^WT Eif5a^K50R Vector
Dox
FLAG
FLAG-eIF5A end-eIF5A
FLAG-eIF5A^Hyp end-eIF5A^Hyp
eIF5A^Hyp targets
POLD1
E2F2
Cyclin D3
PIM3
JUND
AKT1
HTT
SCD1
β-Actin
HSP90α/β
B
shEif5a
Dox
MG132
eIF5A
POLD1
E2F2
Cyclin D3
JUND
HTT
SCD1
250
150
100
75
Ubiquitin
β-Actin
HSP90α/β
C
Active translation
Less active translation
ns
Cell population (%)
Vehicle
4-OHT
D
Vehicle
4-OHT
OP-Puro MFI (× 1,000)
All live cells
Active translation
E
Eμ-Myc;CreER^T2
Dhps^+/+
Dhps^fl/fl
Time (h)
DHPS
eIF5A^Hyp
POLD1
E2F1
E2F2
PIM3
HTT
SCD1
β-Actin
HSP90α/β
F
0 h
72 h
96 h
Rel. expression
Ccne1
Ccne2
Bub1
Kif2c
Cenpe
Top2a
Rpa1
Smc3
Smc4
Smc6
Ppia
Ppib
G
E2F-score
CCNE1
P > 0.05
P = 0.01
P = 0.001
P = 0.0001
P = 1e-05
P = 1e-06
Correlation to EIF5A
H
BrdU-APC
Vehicle
4-OHT
DNA content (DAPI; ×10^3)
Percent cells [%]
Vehicle
4-OHT
G0–G1
S
G2–M
Cell cycle

expression of WT eIF5A but not eIF5A^{K50R} at least partially restored the levels of these eIF5A^{Hyp}-dependent targets (Fig. 6A).

Loss of eIF5A could also conceivably affect proteasome degradation of putative eIF5A^{Hyp} targets. However, treatment with the proteasome inhibitor MG132 did not affect reduction of these targets observed following the knockdown of *Eif5a* (Fig. 6B), indicating that the effects of *Eif5a* knockdown are primarily at the level of translation of these targets.

To confirm these findings in an independent model, we used Eμ-*Myc*;Rosa26-*CreER*^{T2};*Dhps*$^{fl/fl}$ lymphoma cells. First, we evaluated the effects of *Dhps* loss on protein synthesis by assessing O-Propargyl-puromycin (OP-puro) incorporation into nascent polypeptides in vehicle versus 4-OHT–treated cells. Consistent with selective effects on translation (rather than global effects), loss of *Dhps* was associated with modest reductions in OP-Puro incorporation versus control cells (Fig. 6C and D; Supplementary Fig. S6A). Furthermore, similar to the effects of eIF5A knockdown (Fig. 6A and B), immunoblot analyses confirmed that acute *Dhps* deletion provoked reductions in protein levels of most of the same targets, including E2F2, POLD1, PIM3, Cyclin D3, SCD1, and HTT (Fig. 6E; Supplementary Fig. S6B).

In accord with the antiproliferative effects of GC7 on BL and Eμ-*Myc* lymphoma cells (Fig. 2A; Supplementary Fig. S2B), pharmacologic inhibition of hypusination by GC7 also led to reductions in the steady-state levels of both E2F1 and E2F2, as well as to increased cleaved (c)-poly(ADP-ribose) polymerase (cPARP), and these effects were abolished by cotreatment with spermidine (Supplementary Fig. S6C and S6D).

These findings suggested the loss of eIF5A^{Hyp} should compromise the expression of E2F transcription targets that drive transit through the cell cycle. Indeed, analysis of our RNA-seq data revealed differential expression of 188 mouse homologs of the HALLMARK E2F gene set (as defined by MsigDB) upon depletion of eIF5A or DHPS (Supplementary Fig. S6E). This includes reductions in the expression of *bona fide* E2F targets required for cell-cycle progression and DNA replication (e.g., *Ccne2*, *Bub1b*, and *Top2a*; Supplementary Fig. S6F), whereas there were no consistent changes in the expression of *E2f* genes themselves (*E2f1*; $\log_2FC^{sh\text{-}Eif5a} = 0.31$, $q = 0.9$, $\log_2FC^{sh\text{-}Dhps} = -0.71$, $q = 0.84$, *E2f2*; $\log_2FC^{sh\text{-}Eif5a} = -1.62$, $q = 0.52$, $\log_2FC^{sh\text{-}Dhps} = -0.35$, $q = 0.94$). Further, qRT-PCR analyses established time-dependent reductions in these E2F transcription targets following knockout of *Dhps* in Eμ-*Myc*;*Cre-ER*^{T2};*Dhps*$^{fl/fl}$ lymphoma cells (Fig. 6F). Interestingly, there are positive correlations between the expression of *EIF5A* and HALLMARK E2F targets across many human cancer types (Fig. 6G). Thus, in addition to previously reported MYC-E2F interplays (49), our study suggests that eIF5A^{Hyp}, at least in part, contributes to downstream E2F transcription programs by regulating the levels of E2F proteins across a broad spectrum of tumors.

Finally, these findings also suggested that eIF5A^{Hyp} regulates lymphoma cell-cycle progression through the G_1–S transition and DNA replication, which we tested by 5-bromodeoxyuridine (BrdU) incorporation into DNA in Eμ-*Myc*;Rosa26-*CreER*^{T2};*Dhps*$^{fl/fl}$ lymphoma cells treated with 4-OHT versus vehicle. Notably, these studies revealed that *Dhps* loss provoked marked reductions in S-phase and an accumulation of cells in G_1 (Fig. 6H).

Dhps Is Essential for MYC-Driven Lymphomagenesis

Eμ-*Myc* mice develop B-cell lymphoma with nearly 100% penetrance (26). The critical role of eIF5A hypusination in lymphoma maintenance indicated it might also be essential for lymphoma development. To test this hypothesis, we generated an Eμ-*Myc*;CD19-*Cre*;*Dhps*$^{fl/fl}$ mouse, in which *Dhps* is selectively deleted in B lymphocytes via expression of *Cre* recombinase under the control of the B cell–specific *CD19* promoter (Supplementary Fig. S7A), along with littermates lacking only one allele of *Dhps* (Eμ-*Myc*;CD19-*Cre*;*Dhps*$^{fl/+}$) or carrying the *Dhps* gene. Strikingly, long-term evaluation of Eμ-*Myc*;CD19-*Cre*;*Dhps*$^{fl/fl}$ mice revealed that they did not develop lymphoma (Fig. 7A). Indeed, the three mice in this cohort that eventually succumbed to disease evaded Cre-mediated deletion of *Dhps* (Fig. 7B) by silencing *Cre* expression; i.e., these lymphomas retained the Cre recombinase transgene but failed to express the gene (Cre escapees; Fig. 7C). Consequently, *Dhps* is expressed in the Cre escapees (Supplementary Fig. S7B). Thus, there is strong selective pressure for retaining *Dhps* during lymphoma development.

In contrast, there were no statistically significant effects of *Dhps* heterozygosity on overall survival (median survival 95.5 days) versus WT Eμ-*Myc* littermates (median survival 118 days; Fig. 7A). Indeed, Eμ-*Myc*;CD19-*Cre*;*Dhps*$^{fl/+}$ mice tended to have a shorter latency period prior to disease onset, as judged by assessments of splenomegaly, a hallmark of disease in this model (Fig. 7D; Supplementary Fig. S7C). Furthermore, the splenic architecture in this cohort was severely disrupted (e.g., diminished periarteriolar lymphoid sheath), with many large lymphocytes infiltrating the red pulp and lymphoid follicles (Fig. 7E). Thus, *Dhps* heterozygosity appears to accelerate disease onset.

The failure of Eμ-*Myc*;CD19-*Cre*;*Dhps*$^{fl/fl}$ mice to develop lymphoma was not due to effects of *Dhps* loss on B-cell homeostasis, as the proportion of CD19$^+$ B cells in BM isolated

Figure 6. eIF5A^{Hyp} controls translation of regulators of cell-cycle progression and DNA replication in lymphoma. **A,** Immunoblot analyses of the indicated proteins in Eμ-*Myc*;Rosa26-*rtTA* lymphoma cells inducibly expressing only sh-*Eif5a* or sh-*Eif5a* plus either *Eif5a*^{WT} or *Eif5a*^{K50R}, or the vector alone, following Dox treatment for 84 hours. Although β-Actin was identified as a TE^{low} gene following eIF5A or DHPS knockdown, the levels of β-Actin are unaffected by immunoblot analysis. HSP90α/β served as a second control. **B,** Immunoblot analyses of the indicated eIF5A^{Hyp} target proteins in Eμ-*Myc*;Rosa26-rt*TA*^{2} cells expressing sh-*Eif5a* with or without treatment with the proteasome inhibitor MG132 (10 μmol/L for 4 hours). **C,** Nascent polypeptide synthesis evaluated by OP-puro incorporation showing cell population (%) undergoing active translation in Eμ-*Myc*;*CreER*^{T2};*Dhps*$^{fl/fl}$ cells treated with 4-OHT (72 hours; $n = 3$). **D,** MFI showing OP-puro incorporation in actively translating Eμ-*Myc*;*CreER*^{T2};*Dhps*$^{fl/fl}$ cells ($n = 3$). **E,** Time-course immunoblot analyses of the indicated proteins in Eμ-*Myc*;CreER^{T2};*Dhps*$^{fl/fl}$ lymphoma before and following deletion of *Dhps*. **F,** Relative mRNA expression of E2F target genes at the indicated time points following *Dhps* deletion in Eμ-*Myc*;CreER^{T2};*Dhps*$^{fl/fl}$ cells, as analyzed by qRT-PCR ($n = 3$). Housekeeping genes *Ppia* and *Ppib* served as controls. **G,** Correlation between *EIF5A* and HALLMARK E2F target gene sets (MsigDB, red circles) and *CCNE1* expression (blue circles) across TCGA data sets. E2F score is the PC1 from a principal component analysis. **H,** BrdU incorporation assays showing effects of *Dhps* loss on DNA synthesis in Eμ-*Myc*;Cre-ER^{T2};*Dhps*$^{fl/fl}$ lymphoma treated with 4-OHT (72 hours; top) and quantification of cells at different cell-cycle phases (bottom; $n = 3$). Levels of significance determined by unpaired *t* tests in **C**, **D**, **F**, and **H** are indicated as follows: ns, not significant; *, $P < 0.05$; **, $P < 0.01$; ***, $P < 0.001$; ****, $P < 0.0001$. Error bar indicates mean ± SD.

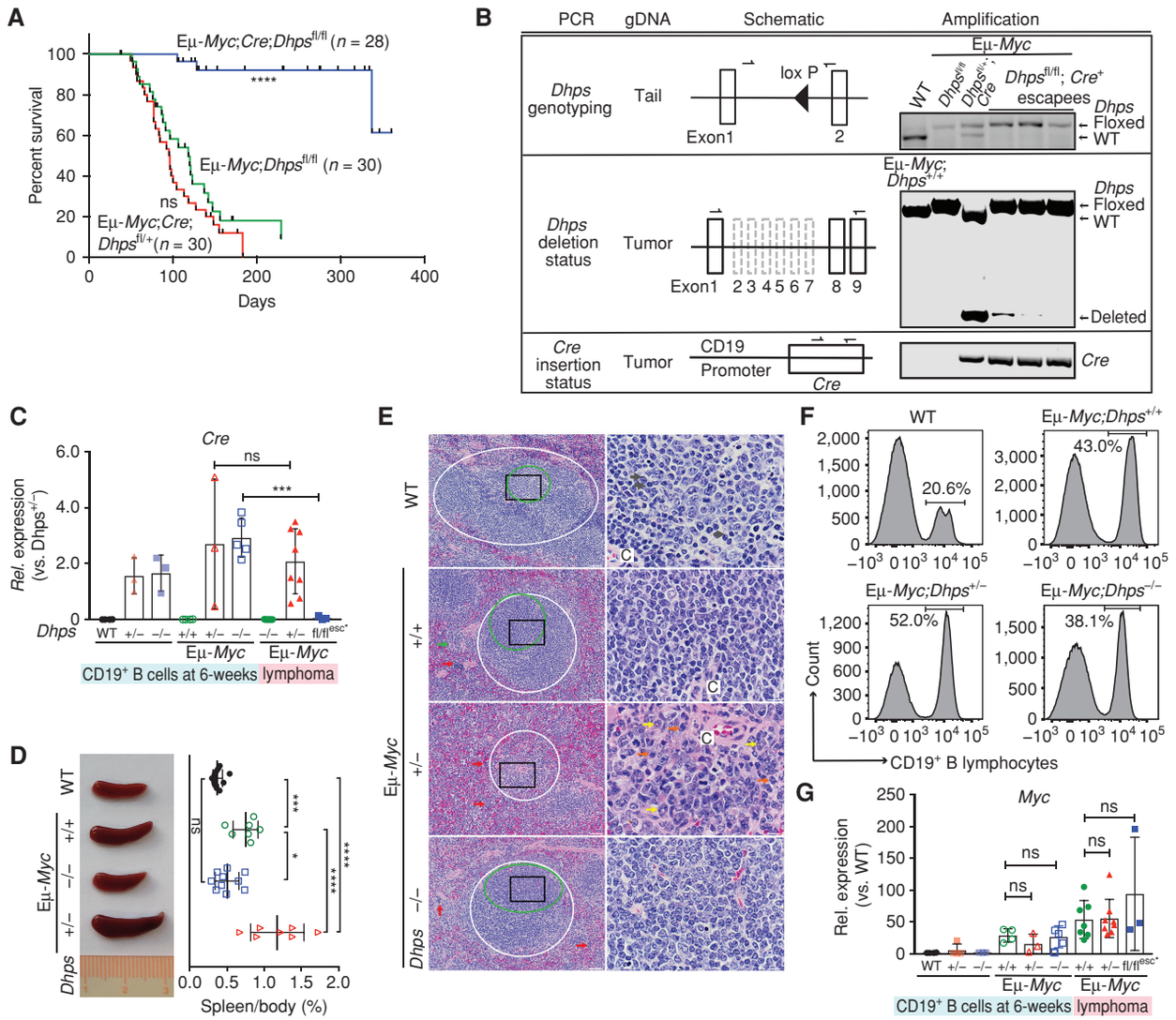

Figure 7. *Dhps* is essential for the development of MYC-driven lymphoma. **A,** Kaplan–Meier curves showing survival of Eμ-*Myc*;CD19-*Cre*;*Dhps*$^{fl/fl}$, Eμ-*Myc*;CD19-*Cre*;*Dhps*$^{fl/+}$, and Eμ-*Myc*;*Dhps*$^{fl/fl}$ mice. **B,** *Dhps* deletion and *Cre* knock-in status, as determined by genomic PCR of the indicated tissues or tumor samples. **C,** *Cre* expression in CD19$^+$ B cells from 6-week-old WT, CD19-Cre;*Dhps*$^{fl/+}$ (hereafter *Dhps*$^{+/-}$), and CD19-Cre;*Dhps*$^{fl/fl}$ (*Dhps*$^{-/-}$); and from preneoplastic and malignant Eμ-*Myc*;CD19-*Cre*;*Dhps* cohorts (Eμ-*Myc*;*Dhps*$^{+/+}$, Eμ-*Myc*;*Dhps*$^{+/-}$, and Eμ-*Myc*;*Dhps*$^{-/-}$) and the 3 Cre escapees (fl/fl^{esc*}), as determined by qRT-PCR ($n \geq 3$ mice). Fold change was calculated relative to *Cre* levels in *Dhps*$^{\pm}$ B cells. **D,** Left, representative images; right, the weight of spleens (normalized to total body weight) from indicated 6-week-old mice ($n > 7$ for each cohort). **E,** Hematoxylin and eosin (H&E) staining of spleens from indicated 7-week-old mice. Periarteriolar lymphoid sheaths (PALS) and germinal centers are shown in white and green circles, respectively. Red, green, yellow, gray, and blue arrows indicate erythroid precursors, megakaryocytes, maturing granulocytic precursors, small lymphocytes, and large lymphocytes, respectively. Central arteriole is indicated as **C**. Black box in the left panels shows the area magnified in the right panels; scale bars, left and right, 50 μm and 10 μm, respectively. **F,** Representative CD19$^+$ B-cell profiles of BM-derived lymphocytes of indicated 6-week-old mice. **G,** *Myc* expression in CD19$^+$ B lymphocytes from indicated 6-week-old littermates, and from preneoplastic and malignant Eμ-*Myc*;CD19-Cre;*Dhps* cohorts (+/+, +/−, and −/−; $n \geq 3$). (*continued on following page*)

from Eμ-*Myc*;CD19-*Cre*;*Dhps*$^{fl/fl}$ mice actually exceeded those present in aged-matched (6-week) littermate WT mice (Fig. 7F). *Dhps* loss also had no effect on the elevated expression of the *Myc* mRNA or protein in preneoplastic Eμ-*Myc* B cells (Fig. 7G; Supplementary Fig. S7D).

Interestingly, morphologic analyses of BM, where disease arises in Eμ-*Myc* mice, revealed that Eμ-*Myc*;CD19-*Cre*;*Dhps*$^{fl/fl}$ mice were similar to their premalignant Eμ-*Myc* littermates, where there were increased numbers of large lymphocytes (Supplementary Fig. S7E), likely due to proliferative activity induced by MYC. However, we observed that the percentage of CD19$^+$ B cells in BM lymphocytes isolated from Eμ-*Myc*;CD19-*Cre*;*Dhps*$^{fl/fl}$ mice was consistently lower than that of their premalignant Eμ-*Myc* littermates, whereas the BM of *Dhps* heterozygous Eμ-*Myc*;CD19-*Cre*;*Dhps*$^{fl/+}$ mice was even more dominated by B cells (Fig. 7F). Moreover, phenotypically, Eμ-*Myc*;CD19-*Cre*;*Dhps*$^{fl/fl}$ mice failed to develop splenomegaly (Fig. 7D) and the spleens of these mice retained their normal architecture (Fig. 7E), indicating *Dhps* loss abolishes progression to the malignant state.

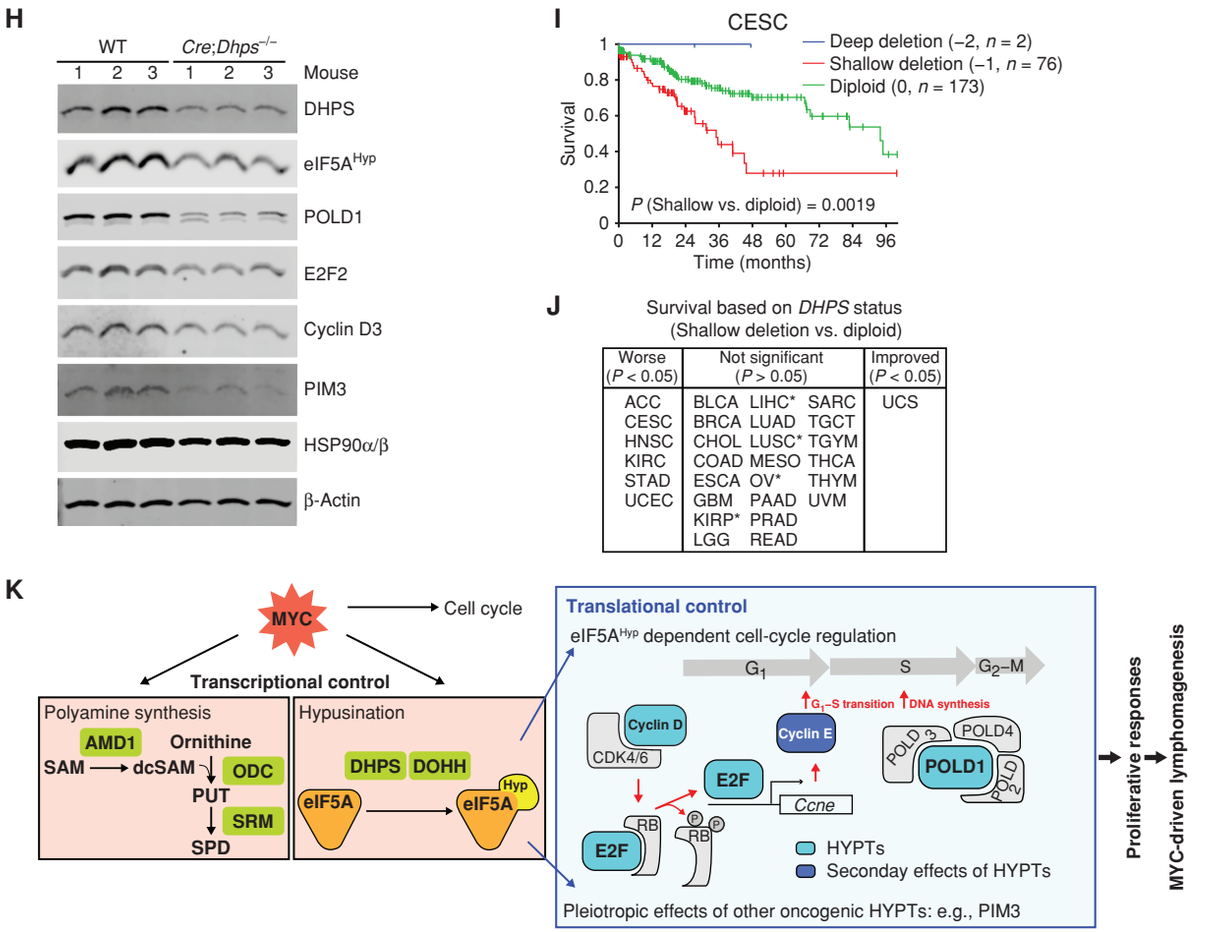

Figure 7. ***(Continued)*** **H,** Immunoblot analyses of identified eIF5A^{Hyp} targets in CD19^{+} B lymphocytes from CD19-Cre;*Dhps*$^{fl/fl}$ and WT littermates ($n = 3$). **I,** Kaplan–Meier curves showing survival of cervical squamous cell carcinoma (CESC) based on *DHPS* copy-number status. **J,** Overall survival based on *DHPS* copy number (shallow deletion vs. diploid). TCGA cancer types in the middle panel that are associated with trends toward worse survival are marked as * ($P < 0.1$). **K,** Model for roles of eIF5A^{Hyp} in MYC-driven lymphoma. The requirement for eIF5A^{Hyp} for Eμ-*Myc* B-cell growth and malignant conversion is associated with MYC-induced hyperactivation of the polyamine–hypusine circuit and eIF5A^{Hyp}-dependent translation of targets such as E2F and POLD1 (turquoise boxes). Cyclin E (blue box) is the transcription target of E2F. HYPTs, eIF5A^{Hyp} targets; PUT, putrescine; SPD, spermidine; SAM, S-adenosylmethionine; dcSAM, decarboxy SAM. Levels of significance determined by Mantel–Cox log-rank test (**A**) and (**I**), unpaired *t* tests (**C**), or Dunnett multiple comparison (**D**) and (**G**) are indicated as follows: ns, not significant; *, $P < 0.05$; **, $P < 0.01$; ***, $P < 0.001$; ****, $P < 0.0001$. Error bar indicates mean ± SD.

Finally, to confirm that key eIF5A^{Hyp} targets identified in Eμ-*Myc* lymphomas (Fig. 6) are dependent upon eIF5A^{Hyp} in B cells *in vivo*, we analyzed their expression in CD19^{+} B cells from 6-week-old CD19-*Cre*;*Dhps*$^{fl/fl}$ mice versus WT mice. Here as well reductions in DHPS protein are associated with selective reductions in eIF5A^{Hyp} and its targets Cyclin D3, E2F2, POLD1, and PIM3 (Fig. 7H).

DHPS Status Is Associated with Outcomes of Some Cancer Types

The requirement for *Dhps* in MYC-driven lymphomagenesis suggested that *DHPS* deletion status might connote outcomes in human cancer. To test this hypothesis, survival analysis of subclassified patient groups based on *DHPS* copy-number alterations was performed across all available TCGA tumor types. As predicted for a gene that is essential for cancer, the number of patients with tumors having deep (–2) deletion of *DHPS* is exceedingly rare; indeed, only 16 cases exist in the entire TCGA. Moreover, although patient numbers are too small to assess statistical significance, in those rare cases where deep deletion of *DHPS* does occur there is improved patient survival (Fig. 7I; Supplementary Fig. S7F). Finally, similar to the accelerated disease phenotypes manifest in *Dhps* heterozygous Eμ-*Myc* mice (Fig. 7A, D and E), shallow deletion (–1) of *DHPS* was associated with worse patient outcomes in several tumor types, including cervical, head and neck and stomach cancers, and exhibited trends toward worse survival in several tumor types (Fig. 7I and J; Supplementary Table S5).

DISCUSSION

Here, we report the essential roles of the hypusine circuit in the development and maintenance of MYC-driven

lymphoma. Specifically, pharmacologic inhibition, knockdown or knockout of DHPS, or knockdown of eIF5A, compromises the growth and survival of extant lymphoma both *ex vivo* and *in vivo*. Furthermore, *Dhps* is necessary for conversion to the fully malignant state *in vivo*, where the loss of *Dhps* abolishes the development of MYC-driven B-cell lymphoma. Finally, unbiased multiomics approaches revealed that hypusinated eIF5A is a translational regulator of key oncoproteins that drive the cell cycle and MYC's proliferative responses.

Notably, although *Eif5a*, *Dhps*, and *Dohh* are all essential for embryonic development (50–52), and as shown here *Dhps* is essential for MYC-driven lymphomagenesis, *Dhps* loss in Eμ-*Myc*;CD19-Cre;*Dhps*$^{fl/fl}$ mice does not impair the percentage of BM B cells versus those found in WT mice. Collectively, the data support a model whereby increased levels of eIF5A and its DHPS/DOHH-modifying enzymes observed in lymphoma are necessary to sustain the highly anabolic state of a developing or extant tumor, and for the transition to the malignant state, as shown by analyses of the precancerous state of Eμ-*Myc*;CD19-Cre;*Dhps*$^{fl/fl}$ mice.

These findings seemingly contrast with those of others who, using an Eμ-*Myc* hematopoietic stem/progenitor cell transplant model and shRNA screens, have suggested tumor suppressor roles of the polyamine–hypusine circuit in MYC-driven lymphomagenesis, by triggering apoptosis (24). There are two likely explanations for these discrepant findings. First, this could reflect developmental differences in the requirement for this circuit during tumorigenesis, where *Dhps* in our study was deleted specifically in B cells, whereas the aforementioned shRNA knockdown studies suppressed the expression of the circuit throughout the entire hematopoietic system. Second, given that *Dhps* heterozygosity appears to provoke a more aggressive course of disease in Eμ-*Myc* mice, it is possible that partial knockdown of this circuit using shRNA leads to one phenotype—accelerated disease—whereas inactivation of the pathway abolishes the conversion to, and maintenance of, the malignant state. Consistent with the required roles of *Dhps* in the conversion to the malignant state, Cre escapees of *Dhps* deletion via silencing *Cre* expression occur during lymphoma development in Eμ-*Myc*;CD19-*Cre*;*Dhps*$^{fl/fl}$ mice. Thus, there is a clear intrinsic selection against tumor cells lacking the hypusine circuit.

Other evidence also argues for the necessary roles of hypusinated eIF5A in tumorigenesis. eIF5A is one of the most abundant proteins in eukaryotic cells (53), and our analyses establish that, regardless of *MYC* involvement, *EIF5A* levels are higher in most cancer types versus matched normal tissue, consistent with its role as an oncogene. Further, although there is LOH in the region of chromosome 17p that harbors *EIF5A* (and notably *TP53*), our analyses indicate that *EIF5A* expression from such tumors is generally equivalent to or higher than *EIF5A* expression in matched normal tissues.

One surprising finding is that shallow deletion of *DHPS* connotes worse outcomes in some human tumor types, and that lymphoma progression (e.g., splenomegaly onset and mean overall survival) appears more aggressive in Eμ-*Myc*;*Dhps*$^{+/-}$ mice versus Eμ-*Myc* mice. One possibility is that this could reflect compensatory upregulation that has been documented in *Dhps*$^{+/-}$ mice, where there are increased levels of *Dhps* mRNA in tissues of *Dhps*$^{+/-}$ mice versus their WT littermates (52). In support of this notion, we note that there are increased levels of *Dhps* transcripts in some lymphomas that arise in Eμ-*Myc*;*Dhps*$^{+/-}$ mice versus levels of *Dhps* mRNA expressed in lymphomas from Eμ-*Myc*;*Dhps*$^{+/+}$ mice (Supplementary Fig. S7B).

Recent findings indicate that hypusinated eIF5A augments translation elongation, rather than functioning as a core translation factor. Furthermore, in accord with recent findings in *S. cerevisiae* (15), our analysis of TE suggests the requirement for hypusinated eIF5A is not limited to the translation of mRNAs containing polyproline codons. Important issues that remain to be resolved are: what features of mRNA (i.e., newly synthesized polypeptide structure) confer a requirement for eIF5A^{Hyp} for their efficient translation; and why eIF5A^{Hyp}-dependent targets are cell context specific, as distinct targets for eIF5A^{Hyp} have been reported in other models (19, 37).

Increasing evidence indicates deregulation of translation control is a hallmark of cancer (54). However, the repertoire of transcripts that are differentially translated in distinct cancer types is largely unknown, and such data could inform potential drug targets and combination strategies to treat cancer. As noted above, eIF5A^{Hyp} targets appear to vary among different cell types. For example, the translation of the autophagy transcription factor TFEB has been reported to be regulated by eIF5A^{Hyp} in normal B cells (19). However, TFEB expression is suppressed in MYC-overexpressing cancers (55, 56) and TFEB was not found as an eIF5A^{Hyp} target in our study.

Notably, at least in the context of MYC-driven lymphoma, eIF5A^{Hyp} directly or indirectly controls the levels of several key regulators of cell-cycle progression. First, targeting the hypusine circuit compromises the translation of E2F transcription factors that control expression of key cell-cycle genes, including *Ccne* (Cyclin E) that is essential for the G_1–S phase transition of the cell cycle. Second, this circuit also appears to control DNA replication, as translation of POLD1, which appears to have roles in the synthesis of both the lagging and leading strands (47), is also impaired following *Eif5a* or *Dhps* knockdown, and by loss of *Dhps*. Collectively, these findings support a model whereby translational regulation by hypusinated eIF5A regulates MYC-driven proliferative responses at several levels (Fig. 7K).

Enforced MYC overexpression is sufficient to initiate a preneoplastic state, but disease progression requires the acquisition of additional alterations that contribute to neoplastic conversion (57–60). The myriad of mutations that are manifest in aggressive hematologic malignancies, including in MYC-driven lymphoma (2), make these tumors particularly challenging to treat, and they are highly prone to developing resistance. Underscoring this fact, although several downstream targets of MYC have been shown to contribute to lymphoma development in the Eμ-*Myc* model (5, 61–66), to date none of them are absolutely required for disease development as is the case for DHPS. Our findings suggest this profound phenotype is due to the pleiotropic

effects of blocking eIF5A hypusination, which is required for the efficient translation of cooperating oncogenes and critical regulators of the cell cycle (Fig. 7K). As activation of the hypusine circuit is a hallmark of MYC-driven tumors, the development of improved small-molecule inhibitors of DHPS, or of agents that bind to and block eIF5A^{Hyp} function, are attractive therapeutic strategies for translating these findings into the clinic. Indeed, the recent discovery of the DHPS allosteric inhibitor bromobenzothiophene (67) provides a new avenue for targeting this circuit, which is needed given the off-target activities of spermidine mimetic compounds such as GC7 (33).

METHODS

Animals

All animal care and the treatment of animals were in strict accordance with Good Animal Practice as defined by the US Office of Laboratory Animal Welfare and were approved by the Moffitt/University South Florida (USF) Institutional Animal Care and Use Committee (IACUC).

Conditional knockout *Dhps*$^{fl/fl}$ mice (37) were backcrossed for at least 10 generations onto a C57BL/6J (The Jackson Laboratory Stock #000664) background. These were crossed with hemizygous Eμ-*Myc* transgenic mice (26) and knock-in CD19-*Cre* mice to generate Eμ-*Myc*;CD19-*Cre*;*Dhps*$^{fl/fl}$ mice. Eμ-*Myc*;Rosa26-*CreER*^{T2};*Dhps*$^{fl/fl}$ mice were generated by crossing *Dhps*$^{fl/fl}$ mice with Rosa26-*CreER*^{T2} (38) and Eμ-*Myc* transgenic mice (Supplementary Table S6).

Experiments were designed to include both males and females in all groups, and no sex-based bias was detected in the observations reported in this study. Unless otherwise stated in the text, all premalignant Eμ-*Myc* mice and Eμ-*Myc* derivatives were 6 to 7 weeks of age at the time of experimentation.

Cell Lines and Culture

Eμ-*Myc* lymphomas were harvested, homogenized in 1× HBSS buffer, filtered through a 100-μm strainer and cultured as a single-cell suspension in 45% DMEM, 45% IMDM, supplemented with 10% fetal bovine serum (FBS), penicillin/streptomycin (100 U/mL), 4 mmol/L GlutaMax, 25 μmol/L β-mercaptoethanol, 1 mmol/L sodium pyruvate, and 5 ng/mL mouse IL7.

Human Raji, Ramos, and Daudi BL cells were purchased from ATCC and were cultured in RPMI-1640 medium supplemented with 10% FBS and penicillin–streptomycin (100 U/mL) and 4 mmol/L L-glutamine at 37°C, 5% CO_2.

P493-6 human B-lymphoma cells (31) were cultured in RPMI-1640 medium, 10% FBS, 4 mmol/L L-glutamine, and penicillin/streptomycin (100 U/mL) at 37°C, 5% CO_2. To manipulate *MYC* transgene expression in these cells, they were cultured in the presence of tetracycline (Tet, 0.1 μg/mL) for 72 hours, resuspended in media without Tet following washing of cells in medium (3×) to induce *MYC* expression, and cultured for the times indicated.

EcoPack cells were maintained in DMEM with 10% FBS, 2 mmol/L L-glutamine, penicillin/streptomycin (100 U/mL) at 37°C, 5% CO_2.

All cell lines (Supplementary Table S7) were routinely tested for mycoplasma contamination and confirmed to be negative using the Mycoplasma PCR detection kit (iNtRON) and/or MycoAlert mycoplasma detection kit (Lonza).

Bacteria Strains

TOP10 and Stbl3 *E. coli* cells (New England Biolabs) were grown in autoclave-sterilized Luria Bertani broth (Fisher Scientific), in a MAXQ6000 shaker (Thermo Scientific) set at 230 rpm and 37°C.

Human Tissue Specimen Studies

Human BL, DHL, and reactive lymph node patient biopsy samples were used for IHC and hematoxylin and eosin (H&E) staining. Formalin-fixed paraffin-embedded lymphoma (FFPE) biopsies from the patients were sectioned (4-μm) and incubated with anti-MYC, anti-eIF5A, and anti-Hypusine antibody (Supplementary Table S8). Slides were scanned using an OLYMPUS BX51 microscope and photographed using an OLYMPUS DP22 camera.

Ethics Reporting

We and our colleagues obtained written informed consent from the patients agreeing to the use of biopsy tissue for research studies. These studies were performed in accordance with recognized ethical guidelines (e.g., Declaration of Helsinki, CIOMS, Belmont Report, U.S. Common Rule), and this study was approved by an institutional review board (IRB).

Mouse Tissue Samples

Mouse spleens and femurs were collected following humane euthanasia. Spleens were formalin-fixed and paraffin-embedded. Femurs were treated with 70% EtOH and decalcified prior to embedding. Sections were stained with H&E, and the staining was visualized using a microscope with magnifications of 10×, 20×, or 40× (Version 3.0. Leica). Samples were processed, and the staining intensity of slides was evaluated at IDEXX BioAnalytics.

Primary B-cell Isolation

B lymphocytes were isolated from the BM of the indicated mice. BM samples were treated with Gey's solution to lyse red blood cells. B cells were isolated using magnetic beads conjugated with CD19 or B220 antibodies and Miltenyi magnetic separation columns per the manufacturer's instructions.

Immunoblotting

Cells were washed with cold Dulbecco's phosphate buffer saline (PBS), lysed in ARF buffer (50 mmol/L HEPES, pH7.5, 150 mmol/L NaCl, 1 mmol/L EDTA, 2.5 mmol/L EGTA, 0.1% Tween-20) supplemented with 1 mmol/L PMSF, 10 mmol/L β-glycerophosphate, 1 mmol/L NaF, 1 mmol/L $NaVO_4$ phosphatase inhibitor and Complete mini protease inhibitor (Roche), and lysates were sonicated and cleared by centrifugation at 4°C. Total protein was quantified using the MicroBCA Protein Assay, and equal amounts of total proteins were loaded on 6%, 7%, 8%, 10%, 12%, or 15% SDS-polyacrylamide gels, transferred onto nitrocellulose membranes with a tank blotting system, and probed with the indicated primary antibodies specific for the proteins of interest (Supplementary Table S8). Membranes were then incubated with a corresponding fluorophore-conjugated secondary antibody and signals were then detected using Odyssey Fc imaging systems (LI-COR). Reagents used in this study are listed in Supplementary Table S9.

Genomic DNA Preparation

Genomic DNA from tails and lymphomas was extracted using the QIAamp DNA Mini Kit (QIAGEN) per the manufacturer's protocol.

Sanger Sequencing

Plasmid constructs generated in this study were confirmed using Sanger sequencing performed by Eurofins Genomics. To assess the mutation status of *Tp53* in Eμ-*Myc*;Rosa26-rtTA^2 lymphoma cells, the p53 coding region was PCR-amplified using cDNA prepared from these cells, and the fragments were sequenced.

Flow Cytometry Analysis and Cell Sorting

At least 10,000 events were acquired on BD Canto II or BD LSRII Flow Cytometer (BD Biosciences), and data were analyzed using the FlowJo software package (TreeStar). For time-course experiments, Rainbow calibration particles (BD Biosciences) were used to evaluate and calibrate the flow cytometer for each use. Additionally, cell sorting was performed using an Aria flow cytometer (BD Biosciences).

Expression of shRNAs targeting *Renilla* (*Ren*), *Eif5a* or *Dhps* expression in Eμ-*Myc*;Rosa26-*rtTA*^{2} lymphoma cells was accomplished by transducing these lymphoma cells with retroviruses expressing inducible miRE shRNA constructs (Supplementary Table S10), which was assessed by monitoring changes in GFP expression over time. GFP$^+$ cells were isolated by sorting after Dox induction of these shRNAs (0.9 μg/mL) overnight.

Proliferation was assessed in Eμ-*Myc*;Rosa26-*rtTA*^{2} lymphoma cell lines transduced with miRE shRNA constructs using the CellTrace Violet (CTV) Cell Proliferation kit (Thermo Fisher Scientific) according to the manufacturer's protocol. For cell proliferation eIF5A rescue experiments, Eμ-*Myc*;Rosa26-*rtTA*^{2} lymphoma cells expressing t*GFP*-sh*Eif5a*$_{\#1}$ were engineered to also inducibly express either WT FLAG-tagged eIF5A (eIF5A^{WT}) or FLAG-tagged K50R-eIF5A (eIF5A^{K50R}), or the vector alone, which expresses tdTomato from an independent promoter. sh*Eif5a* #1 targets the 3′-UTR of the endogenous *Eif5a* gene; thus, expression of exogenous *Eif5A* is not affected by the shRNA. Once the stable cell lines were established, these cells were labeled with CTV as described above and cultured in the presence or absence of Dox. Cell division status was assessed by flow cytometry at the times indicated.

For analysis of nascent peptide synthesis, OP-Puro (20 μmol/L) was added for 1 hour to Eμ-*Myc*;*Cre-ER*^{T2};*Dhps*$^{fl/fl}$ lymphoma cells that had been treated 4-OHT or ethanol for 3 days. Incorporation of OP-Puro into nascent peptides was assessed by conjugation of AlexaFluor 640 using the Click-iT technology (Thermo Fisher) and flow cytometry.

Analyses of early and late apoptosis of Eμ-*Myc*;*Cre-ER*^{T2};*Dhps*$^{fl/fl}$ lymphoma cells following knockout of *Dhps* were performed by staining with FITC-conjugated Annexin V (BD Biosciences) and propidium iodide.

For cell-cycle analyses of Eμ-*Myc*;*Cre-ER*^{T2};*Dhps*$^{fl/fl}$ lymphoma cells, BrdU incorporation was performed using the BrdU assay kit (BD Biosciences) and DAPI staining according to the manufacturer's protocol.

To analyze CD19$^+$ B-cell populations, following RBC removal, single-cell suspensions from mouse BM were stained using the PE-Cy7 anti-CD19 and Zombie cell viability dye (BioLegend).

Cell Growth Assays

Cell growth was measured by counting cells or by MTT assay (Millipore) daily. Human Raji cells were treated with the indicated concentrations of DFMO or GC7 and MTT assays were performed daily according to the manufacturer's instructions. For cell counting assays, Eμ-*Myc*;Rosa26-*rtTA*^{2} lymphoma cells inducibly expressing miR-30 sh*Eif5a* or a scrambled shRNA were seeded in 6-well plates in the absence or presence of Dox (0.9 μg/mL). Cells were counted at the indicated intervals using trypan blue stain (0.2%) and Cellometer Auto 2000 (Nexcelom Bioscience) per the manufacturer's instructions.

Methocult Colony-Forming Assays

Eμ-*Myc*;Rosa26-*rtTA*^{2} lymphoma cells transduced with retrovirus expressing inducible miRE shRNA targeting mouse *Eif5a*, *Dhps, or Renilla* were treated with Dox and sorted for GFP$^+$ cells. On day 3, the cells were washed with media three times and 1.2×10^3 viable cells were resuspended in 1.1 mL MethoCult medium and cultured in 35-mm 6-well plates (SmartDish, STEMCELL Technology) in the presence or absence of Dox (1.0 μg/mL). The images were captured using an automated STEMvision system (STEMCELL Technology) at days 12 and 18 and colonies were counted manually.

Quantitative Real-time PCR Analysis

RNA was isolated from CD19$^+$ B cells, tumors, or cultured cells using NucleoSpin RNA kit per the manufacturer's instructions. cDNA was generated using an iScript cDNA synthesis kit, and qRT-PCR was performed using iQ SYBR green mix (Bio-Rad) on a CFX96 Touch Real-Time PCR Detection System instrument (Bio-Rad). Data were analyzed using the ΔΔCt method, and data were normalized to the expression of *Ubiquitin* (*Ubc*). Primers are listed in the Sequence Information (Supplementary Table S11).

Generation of shRNA Knockdown and Eif5a-Expressing Eμ-Myc Lymphoma Cell Lines

Retroviruses that inducibly express shRNAs targeting mouse *Eif5a* or *Dhps* were constructed in the following manner. 97-mer oligos containing the shRNA sequences listed in Sequence Information (Supplementary Table S11) were synthesized (IDT), annealed, and cloned into either SIN-TREmiRE30-PIG or miRE shRNA (34) vectors. pRetroX-Tight-FLAG-tagged mouse *Eif5a* plasmid was generated by cloning the *FLAG-Eif5a* PCR fragment into the pRetroX-Tight-MCS-PGK-*tdTomato* vector. The K50R amino acid substitution mutant of eIF5A that is defective for hypusination was generated by site-directed mutagenesis using QuickChange II (Agilent).

EcoPack cells were transfected with the indicated plasmids using the ProFection transfection system (Promega). Retrovirus was collected at day 2, filtered through 0.45-μm filter, and added to mouse Eμ-*Myc*;Rosa26-*rtTA*^{2} lymphoma cells. Spin-infection was then performed at 2,500 rpm for 90 minutes in the presence of IL7 (5 ng/mL) and polybrene (8 ng/mL). After the expansion of cells in culture, transduced cells were isolated by selection in antibiotic (G418) or by cell sorting prior to experimental analyses.

Lymphoma Transplant Studies

To assess the effects of pharmacologic inhibition of ODC or DHPS on lymphoma tumorigenic potential, Eμ-*Myc* lymphoma cells were suspended in PBS, and 1 million cells were injected into the tail veins of 7-week-old C57BL/6J female mice and mice were randomly distributed into three groups (10 mice each). Three days after transplant, mice were treated with GC7 (4 or 20 mg/kg) or vehicle (PBS) via daily i.p. injection until animals reached the endpoint. DFMO was administered in drinking water (1% wt/vol) starting one day after the transplant.

To determine the effects of eIF5A depletion on lymphoma tumorigenic potential, Eμ-*Myc*;Rosa26-rt*TA*^{2} cells engineered to inducibly express shRNAs targeting *Eif5a* or *Renilla* were injected into the tail veins of 7-week-old nude female mice (3.5×10^5 cells/mouse) and mice were randomized into 2 groups. Three days after the transplant, half of these mice were shifted to a Dox chow diet (200 μg/kg), which was given daily until the endpoint.

To evaluate the effects of *Dhps* loss on tumor maintenance, 6-week-old athymic male nude recipient mice were transplanted with Eμ-*Myc*;Rosa26-*CreER*^{T2};*Dhps*$^{fl/fl}$; lymphoma cells that were transduced with pRetroX-Tight-MCS-PGK-*OgNLuc*, which expresses the LSSmOrange-NanoLuc reporter (68). Transduced cells were isolated by sorting for LSSmOrange and were suspended in a 1:1 mixture of PBS and Matrigel (Corning). Cell suspensions (1 million cells) were then subcutaneously implanted in the right flank of 6-week-old male nude mice (The Jackson Laboratory). The greatest longitudinal diameter (L), the transverse diameter (W), and the height (H) were measured daily using calipers, and the tumor volume was calculated using the formula, volume = π/6 (L × W × H; ref. 69). Once a palpable tumor formed, mice (bearing established tumors of ~20 mm^3) were randomly assigned to either tamoxifen or vehicle (corn oil) treatment and were dosed daily by oral gavage (145 mg/kg). 13 Eμ-*Myc*;Rosa26-*CreER*^{T2};*Dhps*$^{fl/fl}$ mice were treated

with tamoxifen or corn oil (for 9 consecutive days). As a control, 6 mice bearing Eμ-*Myc*;*Dhps*$^{+/+}$;Rosa26-*CreER*^{T2} lymphomas were either treated with tamoxifen or corn oil. Luminescence signals were monitored twice a week using IVIS spectrum 200 (PerkinElmer) following i.p. injection of furimazine; 2-furanylmethyl-deoxy-coelenterazine (Promega) and were quantified using Living Image software (PerkinElmer).

Sample Preparation for RNA-seq, Ribosome Profiling, and TMT Multilabeling Mass Spectrometry

Eμ-*Myc*;Rosa26-*rtTA*^{2} lymphoma cells engineered to inducibly express shRNAs targeting *Renilla*, *Eif5a*, or *Dhps* were treated with Dox overnight and GFP$^+$ cells were sorted by flow cytometry. Cells were incubated for a total of 72 hours in the presence of Dox, washed with PBS, and harvested. Total RNA for RNA-seq was isolated with the RNAeasy kit (QIAGEN) with in-column DNase treatment. cDNA libraries were generated using Epicentre ScriptSeq Complete Gold Library Prep (Epicentre Biotechnologies). RNA integrity was verified using Agilent 2100 Bioanalyzer (Agilent Technologies) prior to RNA-seq run (NextSeq 500, 2 × 75 High-Output Run). RNA-seq data shown in Fig. 4 and Supplementary Fig. S4 were analyzed at a gene level (see Analyses of RNA-seq data sets), although RNA-seq data used for TE calculation were analyzed at a transcript level (see Analyses of ribosome profiling data sets). For ribosome profiling, Eμ-*Myc*;Rosa26-*rtTA*^{2} lymphoma cells expressing shRNAs targeting *Renilla*, *Eif5a*, or *Dhps* were simultaneously prepared as described above, treated with cycloheximide for 15 minutes prior to harvest, and washed with PBS. Then, ribosome footprint cDNA libraries were prepared according to the protocol described by Ingolia and colleagues (45). Single-end 1 × 50 bp NextSeq runs were performed.

For time-course TMT proteomics analysis, Eμ-*Myc*;Rosa26-*rtTA*^{2} lymphoma cells that inducibly express shRNAs targeting *Renilla*, *Eif5a*, or *Dhps* were treated with Dox overnight and GFP+ cells were isolated by flow cytometry. Cells were then incubated for a total of 72, 96, or 120 hours in the presence of Dox, washed with PBS, and harvested. Cell pellets were then processed for 10 plex TMT-multilabeling mass spectrometry (44). sh-*Ren* cells without Dox treatment (0 hours) were also included as a control in the 10-plex.

Cells were lysed in denaturing buffer containing 8M urea, 20 mmol/L HEPES (pH 8), 1 mmol/L sodium orthovanadate, 2.5 mmol/L sodium pyrophosphate, and 1 mmol/L β-glycerophosphate. Following the determination of protein concentration using the Bradford assay, the proteins were reduced with 4.5 mmol/L dithiothreitol and alkylated with 10 mmol/L iodoacetamide. Trypsin digestion was carried out at room temperature overnight, and tryptic peptides were then acidified with 1% trifluoroacetic acid (TFA) and desalted with C18 Sep-Pak cartridges according to the manufacturer's procedure. An aliquot (100 μg) of tryptic peptide digest from each sample was labeled with TMT10-plex reagent using the following experimental design where the reporter ion channels are listed in parentheses: sh-*Ren* No-Dox (126), sh-*Ren* Dox-72hr (127N), sh-*Ren* Dox-96hr (127C), sh-*Ren* Dox-120hr (128N), sh-*Eif5a* Dox-72hr (128C), sh-*Eif5a* Dox-96hr (129N), sh-*Eif5a* Dox-120hr (129C), sh-*Dhps* Dox-72hr (130N), sh-*Dhps* Dox-96hr (130C), and sh-*Dhps* Dox-120hr (131). The label incorporation and correct label assignment were verified by LC-MS/MS; spectral counts were used to verify that at least 98% of the identified peptides were TMT labeled for each channel. The 10 samples were pooled and lyophilized.

After lyophilization, the peptides were redissolved in 250 μL of aqueous 20 mmol/L ammonium formate (pH 10.0), which was used as the bRPLC A solvent. The basic pH reversed phase separation was performed on a 4.6 mm ID × 100 mm long column packed with BEH C18 resin, 3.5 μm particle size, 130 Å pore size (XBridge, Waters). The peptides were eluted as follows: 5% B (10% aqueous 5 mmol/L ammonium formate, 90% acetonitrile, pH 10.0) for 10 minutes, 5%–15% B in 5 minutes, 15%–40% B in 47 minutes, 40%–100% B in 5 minutes and 100% B held for 10 minutes, followed by reequilibration at 5% B. The flow rate was 0.6 mL/minute, and 24 concatenated fractions were collected. Peptide fractions were dried by vacuum centrifugation (Speedvac, Thermo).

A nanoflow ultra-high performance liquid chromatograph interfaced with an electrospray benchtop orbitrap mass spectrometer (RSLCnano and Q-Exactive Plus, Thermo) was used for tandem mass spectrometry peptide sequencing experiments. The sample was first loaded onto a precolumn (2 cm ID × 100 μm length packed with C18 reversed phase resin, 5 μm particle size, 100 Å pore size (C18 PepMap100, Thermo) and washed for 8 minutes with aqueous 2% acetonitrile and 0.1% formic acid (LC-MS/MS solvent A). The trapped peptides were separated by a C18 reversed phase analytical column 75 μm ID × 25 cm, 2 μm particle size, and 100 Å pore size (C18 PepMap100, Thermo). The 120-minute gradient was programmed as: 95% solvent A (aqueous 2% acetonitrile + 0.1% formic acid) for 8 minutes, solvent B (aqueous 90% acetonitrile + 0.1% formic acid) from 5% to 38.5% in 90 minutes, then solvent B from 50% to 90% B in 7 minutes and held at 90% for 5 minutes, followed by solvent B from 90% to 5% in 1 minute and reequilibration for 10 minutes. The flow rate on the analytical column was 300 nL/minute. Twenty tandem mass spectra were collected in a data-dependent manner following each survey scan. The resolution settings were 60,000 and 45,000 for MS1 and MS/MS, respectively. The isolation window was 0.8 Th with 0.2 offset.

Analyses of Public Data Sets

Public data sets used in this study are listed in Supplementary Table S12.

Analyses of TCGA PanCanAtlas Data Sets. To compare the expression of *EIF5A*, *EIF5A2*, *DHPS*, and *DOHH* in human malignant tumors (red) and related normal tissues (blue) across publicly available different cancer types, the TCGA PanCanAtlas data sets downloaded from the https://gdc.cancer.gov/about-data/publications/pancanatlas were $\log_2$ transformed. Samples listed in merged_sample_quality_annotations.tsv were removed from further analysis. Following QC, 17 cancer types were used throughout the study based on the availability of normal tissue sample ($n > 5$).

Analyses of copy-number alterations (CAN) were performed using the GISTIC data from the https://gdc.cancer.gov/about-data/publications/pancan-aneuploidy genes whitelisted tsv file. We observed significant overexpression of *EIF5A* in 12 of the aforementioned 17 TCGA cancer types. These 12 cancer types were classified based on *EIF5A* copy-number status; deep (–2), shallow (–1), and diploid (0, WT) and were compared with *EIF5A* $\log_2$ expression of these subgroups with the normal samples.

TCGA survival data were based on the TCGA Pan-Cancer Clinical Data resource (TCGA-CDR) as described by Liu and colleagues (70).

Analyses of GSE12453. Data of BL patients and normal B-cell subsets were extracted from GSE12453 (71). The top 20 overexpressed genes were determined by comparing in BL and normal B-cell subsets using a two-sided *t* test to calculate each *P* value. Log_2 fold change was calculated as mean expression for one group minus mean expression for the other group. A heat map showing expression profiling of genes of the hypusine circuit was generated to compare expression in BL and normal B-cell subsets genes. Significance of each probe was determined by an unpaired *t* test analysis.

Analyses of GSE32239 and GSE33474. To compare the expression of genes involved in the polyamine–hypusine circuit in Eμ-*Myc* mice, we used our published WT B-cell and Eμ-*Myc* data sets: GSE32239, spleen (5) and GSE33474, BM (72). Expression values were first $\log_2$

transformed, and heat maps were generated by MATLAB R2020a. The fold change of expression of probe sets and their significance were determined as described above.

Analyses of GSE15907. To analyze the expression of genes of the hypusine circuit during B-cell development, GSE15907 ImmGen data were downloaded from Gene-Expression Omnibus (GEO) as a Series Matrix File and $\log_2$ transformed (73).

Analyses of RNA-seq Data Sets

Processed raw reads were aligned to mouse genome mm10 using TopHat (v2.0.13; ref. 74). Gene expression was evaluated as read count at gene level with HTSeq (v0.6.1; ref. 75). The data were then normalized, and differential expression between experimental groups was analyzed using DEseq2 (76). Genes were considered to be differentially expressed if $q < 0.05$ (DEG). Expression data were $\log_2$ transformed, $\log_2(x + 1)$, and the relative expression was calculated by removing the mean. Specific comparisons that are shown in Fig. 4 and Supplementary Fig. S4 represent averages calculated from two biological duplicates at the gene levels.

For expression analysis of mouse E2F target genes on the RNA-seq data, HALLMARK E2F target genes (GSEA, 200 human genes) were first mapped to 188 corresponding mouse genes and the first principal component was used to show differential expression between the controls and the *Dhps* or *Eif5a* knockdown samples.

Analyses of Ribosome Profiling Data Sets

Raw Sequence Read Alignment. Single-end sequence reads from three independent runs were merged and clipped for the manually identified adapter: CTGTAGGCACCATCAAT. One base was then trimmed from the 5′ end and 3′ end using FASTX Toolkit (v0.0.13). Reads with 19 or fewer bases were discarded. Approximately 98% of the reads were retained afterward. Reads corresponding to ribosomal RNA (rRNA) sequence were removed by aligning to the mouse ribosomal RNA reference sequence using bowtie2. Resulting reads were aligned to the mouse genome assembly (GRCm38/mm10) using TopHat (v2.0.13; ref. 74). Aligned reads were ordered by name and the total number of reads for a given gene transcript were counted using HTSeq (v0.6.1; ref. 75).

TE Calculation. Transcript expression levels from our RNA-seq experiment and ribosomal densities from the Ribo-seq experiment were normalized using the RPKM method. Pairwise scatter plot and Pearson correlation coefficients were used to assess the agreement and quality of RPKM data between biological replicates. The degree of TE for individual transcripts was then quantified by dividing Ribo-seq RPKM by RNA-seq RPKM. To avoid a zero denominator, we then added a very small number, 1e–10, to all RNA-seq RPKMs. The R LIMMA package (77) was used to perform differential TE analysis. False discovery rate was controlled using Benjamini–Hochberg method for a multiple testing correction in the differential TE analyses. DTTs ($P < 0.05$) that were identified from TE analysis are summarized in Supplementary Table S3.

TE Analysis of Oncogenes and Tumor Suppressor Genes. The general human cancer-related gene list was obtained from the Bushman lab site (http://www.bushmanlab.org/links/genelists). Then, a literature search was performed to search for additional oncogenes and tumor suppressors, especially those that were related to lymphoma. Finally, among these combined human cancer genes, the mouse homologs were identified to generate our mouse cancer gene lists. Among those potential oncogene/tumor suppressor genes, DTTs were then ranked based on their $\log_2$ fold changes in TE (vs. sh-*Ren* cells). Note that genes whose roles have been reported to function as both an oncogene and a tumor suppressor were also included in the list. The oncogene/tumor suppressors that are differentially translated upon depletion of eIF5A or DHPS are listed in Supplementary Table S4.

Analyses of TMT Proteomics Data Sets

MaxQuant (version 1.5.2.8; ref. 78) was used to quantify the TMT reporter ion intensities. Database search was performed using trypsin with up to 2 missed cleavages, modifications included TMT labeling of lysines and peptide *N*-termini, carbamidomethylation of cysteine, and oxidation of methionine. Similar parameters were used for Mascot database searches to support data upload. Further, the intensity from all 10 samples was normalized using the Iterative rank-order normalization (IRON) algorithm (79).

Statistical Analyses of Experimental Data Sets

Statistical analyses were performed using GraphPad Prism 7 and MATLAB and a *P* value of less than 0.05 was considered statistically significant. The levels of significance were determined using an unpaired two-tailed Student *t* test or ANOVA, and *P* values are provided in the figures or the legends. Error bars presented in the figures indicate the mean ± SD unless otherwise specified. The statistical parameters are described in the individual figure legends. For survival analyses, overall survival was estimated with the Kaplan–Meier method and compared using a log-rank test.

Data Availability

This study did not generate any original code. Software and algorithms used in this study are listed in Supplementary Table S13. RNA-seq and Ribo-seq data sets were deposited in the GEO, GSE190669 and GSE190670, respectively. TMT multilabeling mass spectrometry data were deposited to the ProteomeXchange Consortium via the PRIDE partner repository with the data set identifier Project accession: PXD031361 and Project DOI: 10.6019/PXD031361.

Authors' Disclosures

R.G. Mirmira reports grants from NIH during the conduct of the study. J.L. Cleveland reports grants from NCI/NIH and other support from Cortner-Couch Endowed Chair for Cancer Research from the University of South Florida during the conduct of the study. No disclosures were reported by the other authors.

Authors' Contributions

S. Nakanishi: Conceptualization, resources, data curation, formal analysis, supervision, validation, investigation, visualization, methodology, writing–original draft, writing–review and editing. **J. Li:** Data curation, software, formal analysis, visualization, methodology, writing–original draft. **A.E. Berglund:** Data curation, software, formal analysis, visualization, methodology, writing–original draft, writing–review and editing. **Y. Kim:** Data curation, software, formal analysis, visualization, methodology, writing–original draft. **Y. Zhang:** Data curation, software, formal analysis, methodology, writing–original draft. **L. Zhang:** Data curation, formal analysis, methodology, writing–original draft. **C. Yang:** Data curation. **J. Song:** Resources. **R.G. Mirmira:** Resources. **J.L. Cleveland:** Conceptualization, resources, data curation, formal analysis, supervision, funding acquisition, validation, investigation, visualization, methodology, writing–original draft, project administration, writing–review and editing.

Acknowledgments

We sincerely thank Dr. Nicholas Ingolia for technical advice on ribosome profiling analyses and critical review of this study. We also thank Dr. Srikumar Chellappan and Sathya Puthamveettil (Scripps Research) for critical review of this study. We also

thank the Genomics Core of Scripps Research and the Molecular Genomics Core of Moffitt Cancer Center (MCC) for RNA-seq, the Proteomics and Metabolomics Core (MCC) for TMT analyses, the Tissue Core (MCC) for IHC analyses, the Flow Cytometry Core (MCC) for cell sorting and technical advice, and the Biostatistics and Bioinformatics Shared Resource for bioinformatics support. The miRE shRNA plasmid was a kind gift from Dr. Johannes Zuber (IMP, Austria). We also thank Dr. Maier Bernhard for providing the eIF5A^{Hyp} antibody and are grateful to Moffitt/USF Department of Comparative Medicine for exceptional animal care and mouse husbandry. This work was supported by R01 grants CA100603 and CA241713 (J.L. Cleveland), by NCI Comprehensive Cancer Center Grant P30 CA076292, by the Cortner-Couch Endowed Chair for Cancer Research from the University of South Florida School of Medicine (J.L. Cleveland), and by monies from the State of Florida to the H. Lee Moffitt Cancer Center and Research Institute. This work was also supported R01 grants DK124906 and DK060581 (R.G. Mirmira), and by the Diabetes Research Center Grant P30 DK020595 (R.G. Mirmira).

The publication costs of this article were defrayed in part by the payment of publication fees. Therefore, and solely to indicate this fact, this article is hereby marked "advertisement" in accordance with 18 USC section 1734.

Note

Supplementary data for this article are available at Blood Cancer Discovery Online (https://bloodcancerdiscov.aacrjournals.org/).

Received September 28, 2022; revised March 1, 2023; accepted April 13, 2023; published first April 18, 2023.

REFERENCES

1. Gabay M, Li Y, Felsher DW. MYC activation is a hallmark of cancer initiation and maintenance. Cold Spring Harb Perspect Med 2014;4:a014241.
2. Reddy A, Zhang J, Davis NS, Moffitt AB, Love CL, Waldrop A, et al. Genetic and functional drivers of diffuse large B cell lymphoma. Cell 2017;171:481–94.
3. Durie BG, Salmon SE, Russell DH. Polyamines as markers of response and disease activity in cancer chemotherapy. Cancer Res 1977;37:214–21.
4. Russell DH. Increased polyamine concentrations in the urine of human cancer patients. Nat New Biol 1971;233:144–5.
5. Nilsson JA, Keller UB, Baudino TA, Yang C, Norton S, Old JA, et al. Targeting ornithine decarboxylase in Myc-induced lymphomagenesis prevents tumor formation. Cancer Cell 2005;7:433–44.
6. Rounbehler RJ, Li W, Hall MA, Yang C, Fallahi M, Cleveland JL. Targeting ornithine decarboxylase impairs development of MYCN-amplified neuroblastoma. Cancer Res 2009;69:547–53.
7. Hogarty MD, Norris MD, Davis K, Liu X, Evageliou NF, Hayes CS, et al. ODC1 is a critical determinant of MYCN oncogenesis and a therapeutic target in neuroblastoma. Cancer Res 2008;68:9735–45.
8. Simoneau AR, Gerner EW, Nagle R, Ziogas A, Fujikawa-Brooks S, Yerushalmi H, et al. The effect of difluoromethylornithine on decreasing prostate size and polyamines in men: results of a year-long phase IIb randomized placebo-controlled chemoprevention trial. Cancer Epidemiol Biomarkers Prev 2008;17:292–9.
9. Raj KP, Zell JA, Rock CL, McLaren CE, Zoumas-Morse C, Gerner EW, et al. Role of dietary polyamines in a phase III clinical trial of difluoromethylornithine (DFMO) and sulindac for prevention of sporadic colorectal adenomas. Br J Cancer 2013;108:512–8.
10. Casero RA Jr, Marton LJ. Targeting polyamine metabolism and function in cancer and other hyperproliferative diseases. Nat Rev Drug Discov 2007;6:373–90.
11. Miller-Fleming L, Olin-Sandoval V, Campbell K, Ralser M. Remaining mysteries of molecular biology: the role of polyamines in the cell. J Mol Biol 2015;427:3389–406.
12. Park MH, Cooper HL, Folk JE. The biosynthesis of protein-bound hypusine (N epsilon -(4-amino-2-hydroxybutyl)lysine). Lysine as the amino acid precursor and the intermediate role of deoxyhypusine (N epsilon -(4-aminobutyl)lysine). J Biol Chem 1982;257:7217–22.
13. Benne R, Brown-Luedi ML, Hershey JW. Purification and characterization of protein synthesis initiation factors eIF-1, eIF-4C, eIF-4D, and eIF-5 from rabbit reticulocytes. J Biol Chem 1978;253:3070–7.
14. Saini P, Eyler DE, Green R, Dever TE. Hypusine-containing protein eIF5A promotes translation elongation. Nature 2009;459:118–21.
15. Schuller AP, Wu CC, Dever TE, Buskirk AR, Green R. eIF5A functions globally in translation elongation and termination. Mol Cell 2017;66:194–205.
16. Manjunath H, Zhang H, Rehfeld F, Han J, Chang TC, Mendell JT. Suppression of ribosomal pausing by eIF5A Is necessary to maintain the fidelity of start codon selection. Cell Rep 2019;29:3134–46.
17. Gutierrez E, Shin BS, Woolstenhulme CJ, Kim JR, Saini P, Buskirk AR, et al. eIF5A promotes translation of polyproline motifs. Mol Cell 2013;51:35–45.
18. Liang Y, Piao C, Beuschel CB, Toppe D, Kollipara L, Bogdanow B, et al. eIF5A hypusination, boosted by dietary spermidine, protects from premature brain aging and mitochondrial dysfunction. Cell Rep 2021;35:108941.
19. Zhang H, Alsaleh G, Feltham J, Sun Y, Napolitano G, Riffelmacher T, et al. Polyamines control eIF5A hypusination, TFEB translation, and autophagy to reverse B cell senescence. Mol Cell 2019;76:110–25.
20. Puleston DJ, Buck MD, Klein Geltink RI, Kyle RL, Caputa G, O'Sullivan D, et al. Polyamines and eIF5A hypusination modulate mitochondrial respiration and macrophage activation. Cell Metab 2019;30:352–63.
21. Anderson-Baucum E, Pineros AR, Kulkarni A, Webb-Robertson BJ, Maier B, Anderson RM, et al. Deoxyhypusine synthase promotes a pro-inflammatory macrophage phenotype. Cell Metab 2021;33:1883–93.
22. Nakanishi S, Cleveland JL. Targeting the polyamine-hypusine circuit for the prevention and treatment of cancer. Amino Acids 2016;48:2353–62.
23. Fujimura K, Wright T, Strnadel J, Kaushal S, Metildi C, Lowy AM, et al. A hypusine-eIF5A-PEAK1 switch regulates the pathogenesis of pancreatic cancer. Cancer Res 2014;74:6671–81.
24. Scuoppo C, Miething C, Lindqvist L, Reyes J, Ruse C, Appelmann I, et al. A tumour suppressor network relying on the polyamine-hypusine axis. Nature 2012;487:244–8.
25. Liu Y, Chen C, Xu Z, Scuoppo C, Rillahan CD, Gao J, et al. Deletions linked to TP53 loss drive cancer through p53-independent mechanisms. Nature 2016;531:471–5.
26. Adams JM, Harris AW, Pinkert CA, Corcoran LM, Alexander WS, Cory S, et al. The c-myc oncogene driven by immunoglobulin enhancers induces lymphoid malignancy in transgenic mice. Nature 1985;318:533–8.
27. El-Ghammaz AM, Abdelwahed E, Mostafa NN, Mansour DA. De novo deletion 17p13.1 as a predictor for disease progression in chronic lymphocytic leukemia. Clin Exp Med 2015;15:493–9.
28. Seifert H, Mohr B, Thiede C, Oelschlagel U, Schakel U, Illmer T, et al. The prognostic impact of 17p (p53) deletion in 2272 adults with acute myeloid leukemia. Leukemia 2009;23:656–63.
29. Baker SJ, Fearon ER, Nigro JM, Hamilton SR, Preisinger AC, Jessup JM, et al. Chromosome 17 deletions and p53 gene mutations in colorectal carcinomas. Science 1989;244:217–21.
30. Fields AP, Justilien V, Murray NR. The chromosome 3q26 OncCassette: a multigenic driver of human cancer. Adv Biol Regul 2016;60:47–63.
31. Pajic A, Spitkovsky D, Christoph B, Kempkes B, Schuhmacher M, Staege MS, et al. Cell cycle activation by c-myc in a Burkitt lymphoma model cell line. Int J Cancer 2000;87:787–93.
32. Jakus J, Wolff EC, Park MH, Folk JE. Features of the spermidine-binding site of deoxyhypusine synthase as derived from inhibition

studies. Effective inhibition by bis- and mono-guanylated diamines and polyamines. J Biol Chem 1993;268:13151–9.
33. Oliverio S, Corazzari M, Sestito C, Piredda L, Ippolito G, Piacentini M. The spermidine analogue GC7 (N1-guanyl-1,7-diamineoheptane) induces autophagy through a mechanism not involving the hypusination of eIF5A. Amino Acids 2014;46:2767–76.
34. Fellmann C, Hoffmann T, Sridhar V, Hopfgartner B, Muhar M, Roth M, et al. An optimized microRNA backbone for effective single-copy RNAi. Cell Rep 2013;5:1704–13.
35. Torrelio BM, Paz MA, Gallop PM. The formation and stability of the hypusine containing protein in Chinese hamster ovary cells. Biochem Biophys Res Commun 1987;145:1335–41.
36. Gao J, Aksoy BA, Dogrusoz U, Dresdner G, Gross B, Sumer SO, et al. Integrative analysis of complex cancer genomics and clinical profiles using the cBioPortal. Sci Signal 2013;6:pl1.
37. Levasseur EM, Yamada K, Pineros AR, Wu W, Syed F, Orr KS, et al. Hypusine biosynthesis in beta cells links polyamine metabolism to facultative cellular proliferation to maintain glucose homeostasis. Sci Signal 2019;12:eaax0715.
38. Ventura A, Kirsch DG, McLaughlin ME, Tuveson DA, Grimm J, Lintault L, et al. Restoration of p53 function leads to tumour regression in vivo. Nature 2007;445:661–5.
39. Tripathi S, Pohl MO, Zhou Y, Rodriguez-Frandsen A, Wang G, Stein DA, et al. Meta- and orthogonal integration of influenza "OMICs" data defines a role for UBR4 in virus budding. Cell Host Microbe 2015;18:723–35.
40. Sabo A, Kress TR, Pelizzola M, de Pretis S, Gorski MM, Tesi A, et al. Selective transcriptional regulation by Myc in cellular growth control and lymphomagenesis. Nature 2014;511:488–92.
41. Kelemen K, Braziel RM, Gatter K, Bakke TC, Olson S, Fan G. Immunophenotypic variations of Burkitt lymphoma. Am J Clin Pathol 2010;134:127–38.
42. Masir N, Marafioti T, Jones M, Natkunam Y, Rudiger T, Hansmann ML, et al. Loss of CD19 expression in B-cell neoplasms. Histopathology 2006;48:239–46.
43. Ingolia NT, Ghaemmaghami S, Newman JR, Weissman JS. Genome-wide analysis in vivo of translation with nucleotide resolution using ribosome profiling. Science 2009;324:218–23.
44. Thompson A, Schafer J, Kuhn K, Kienle S, Schwarz J, Schmidt G, et al. Tandem mass tags: a novel quantification strategy for comparative analysis of complex protein mixtures by MS/MS. Anal Chem 2003;75:1895–904.
45. Ingolia NT, Brar GA, Rouskin S, McGeachy AM, Weissman JS. The ribosome profiling strategy for monitoring translation in vivo by deep sequencing of ribosome-protected mRNA fragments. Nat Protoc 2012;7:1534–50.
46. Zheng Z, Diamond MI. Huntington disease and the huntingtin protein. Prog Mol Biol Transl Sci 2012;107:189–214.
47. Nick McElhinny SA, Stith CM, Burgers PM, Kunkel TA. Inefficient proofreading and biased error rates during inaccurate DNA synthesis by a mutant derivative of Saccharomyces cerevisiae DNA polymerase delta. J Biol Chem 2007;282:2324–32.
48. Xie H, Tang CH, Song JH, Mancuso A, Del Valle JR, Cao J, et al. IRE1alpha RNase-dependent lipid homeostasis promotes survival in Myc-transformed cancers. J Clin Invest 2018;128:1300–16.
49. Leone G, Sears R, Huang E, Rempel R, Nuckolls F, Park CH, et al. Myc requires distinct E2F activities to induce S phase and apoptosis. Mol Cell 2001;8:105–13.
50. Nishimura K, Lee SB, Park JH, Park MH. Essential role of eIF5A-1 and deoxyhypusine synthase in mouse embryonic development. Amino Acids 2012;42:703–10.
51. Sievert H, Pallmann N, Miller KK, Hermans-Borgmeyer I, Venz S, Sendoel A, et al. A novel mouse model for inhibition of DOHH-mediated hypusine modification reveals a crucial function in embryonic development, proliferation and oncogenic transformation. Dis Model Mech 2014;7:963–76.
52. Pallmann N, Braig M, Sievert H, Preukschas M, Hermans-Borgmeyer I, Schweizer M, et al. Biological relevance and therapeutic potential of the hypusine modification system. J Biol Chem 2015;290:18343–60.
53. Kulak NA, Pichler G, Paron I, Nagaraj N, Mann M. Minimal, encapsulated proteomic-sample processing applied to copy-number estimation in eukaryotic cells. Nat Methods 2014;11:319–24.
54. Truitt ML, Ruggero D. New frontiers in translational control of the cancer genome. Nat Rev Cancer 2016;16:288–304.
55. Annunziata I, van de Vlekkert D, Wolf E, Finkelstein D, Neale G, Machado E, et al. MYC competes with MiT/TFE in regulating lysosomal biogenesis and autophagy through an epigenetic rheostat. Nat Commun 2019;10:3623.
56. Yun S, Vincelette ND, Yu X, Watson GW, Fernandez MR, Yang C, et al. TFEB links MYC signaling to epigenetic control of myeloid differentiation and acute myeloid leukemia. Blood Cancer Discov 2021;2:162–85.
57. Lefebure M, Tothill RW, Kruse E, Hawkins ED, Shortt J, Matthews GM, et al. Genomic characterisation of Emu-Myc mouse lymphomas identifies Bcor as a Myc co-operative tumour-suppressor gene. Nat Commun 2017;8:14581.
58. Eischen CM, Weber JD, Roussel MF, Sherr CJ, Cleveland JL. Disruption of the ARF-Mdm2-p53 tumor suppressor pathway in Myc-induced lymphomagenesis. Genes Dev 1999;13:2658–69.
59. Gorrini C, Squatrito M, Luise C, Syed N, Perna D, Wark L, et al. Tip60 is a haplo-insufficient tumour suppressor required for an oncogene-induced DNA damage response. Nature 2007;448:1063–7.
60. Schmitt CA, McCurrach ME, de Stanchina E, Wallace-Brodeur RR, Lowe SW. INK4a/ARF mutations accelerate lymphomagenesis and promote chemoresistance by disabling p53. Genes Dev 1999;13:2670–7.
61. Rempel RE, Mori S, Gasparetto M, Glozak MA, Andrechek ER, Adler SB, et al. A role for E2F activities in determining the fate of Myc-induced lymphomagenesis. PLoS Genet 2009;5:e1000640.
62. Baudino TA, Maclean KH, Brennan J, Parganas E, Yang C, Aslanian A, et al. Myc-mediated proliferation and lymphomagenesis, but not apoptosis, are compromised by E2f1 loss. Mol Cell 2003;11:905–14.
63. Keller UB, Old JB, Dorsey FC, Nilsson JA, Nilsson L, MacLean KH, et al. Myc targets Cks1 to provoke the suppression of p27Kip1, proliferation and lymphomagenesis. EMBO J 2007;26:2562–74.
64. Lin CJ, Nasr Z, Premsrirut PK, Porco JA Jr, Hippo Y, Lowe SW, et al. Targeting synthetic lethal interactions between Myc and the eIF4F complex impedes tumorigenesis. Cell Rep 2012;1:325–33.
65. Farria AT, Plummer JB, Salinger AP, Shen J, Lin K, Lu Y, et al. Transcriptional activation of MYC-induced genes by GCN5 promotes B-cell lymphomagenesis. Cancer Res 2020;80:5543–53.
66. Zwolinska AK, Heagle Whiting A, Beekman C, Sedivy JM, Marine JC. Suppression of Myc oncogenic activity by nucleostemin haploinsufficiency. Oncogene 2012;31:3311–21.
67. Tanaka Y, Kurasawa O, Yokota A, Klein MG, Ono K, Saito B, et al. Discovery of novel allosteric inhibitors of deoxyhypusine synthase. J Med Chem 2020;63:3215–26.
68. Schaub FX, Reza MS, Flaveny CA, Li W, Musicant AM, Hoxha S, et al. Fluorophore-NanoLuc BRET reporters enable sensitive in vivo optical imaging and flow cytometry for monitoring tumorigenesis. Cancer Res 2015;75:5023–33.
69. Tomayko MM, Reynolds CP. Determination of subcutaneous tumor size in athymic (nude) mice. Cancer Chemother Pharmacol 1989;24:148–54.
70. Liu J, Lichtenberg T, Hoadley KA, Poisson LM, Lazar AJ, Cherniack AD, et al. An integrated TCGA pan-cancer clinical data resource to drive high-quality survival outcome analytics. Cell 2018;173:400–16.
71. Brune V, Tiacci E, Pfeil I, Doring C, Eckerle S, van Noesel CJ, et al. Origin and pathogenesis of nodular lymphocyte-predominant Hodgkin lymphoma as revealed by global gene expression analysis. J Exp Med 2008;205:2251–68.
72. Rounbehler RJ, Fallahi M, Yang C, Steeves MA, Li W, Doherty JR, et al. Tristetraprolin impairs myc-induced lymphoma and abolishes the malignant state. Cell 2012;150:563–74.
73. Heng TS, Painter MW; Immunological Genome Project C. The immunological genome project: networks of gene expression in immune cells. Nat Immunol 2008;9:1091–4.
74. Trapnell C, Pachter L, Salzberg SL. TopHat: discovering splice junctions with RNA-Seq. Bioinformatics 2009;25:1105–11.

75. Anders S, Pyl PT, Huber W. HTSeq–a Python framework to work with high-throughput sequencing data. Bioinformatics 2015;31:166–9.
76. Love MI, Huber W, Anders S. Moderated estimation of fold change and dispersion for RNA-seq data with DESeq2. Genome Biol 2014;15:550.
77. Ritchie ME, Phipson B, Wu D, Hu Y, Law CW, Shi W, et al. limma powers differential expression analyses for RNA-sequencing and microarray studies. Nucleic Acids Res 2015;43:e47.
78. Cox J, Mann M. MaxQuant enables high peptide identification rates, individualized p.p.b.-range mass accuracies and proteome-wide protein quantification. Nat Biotechnol 2008;26:1367–72.
79. Welsh EA, Eschrich SA, Berglund AE, Fenstermacher DA. Iterative rank-order normalization of gene expression microarray data. BMC Bioinformatics 2013;14:153.